ORIGINAL ARTICLE

Journal of Cachexia, Sarcopenia and Muscle 2021; **12**: 456–475
Published online 17 February 2021 in Wiley Online Library (wileyonlinelibrary.com) **DOI:** 10.1002/jcsm.12684

Multi-compartment metabolomics and metagenomics reveal major hepatic and intestinal disturbances in cancer cachectic mice

Sarah A. Pötgens[1], Morgane M. Thibaut[1], Nicolas Joudiou[2], Martina Sboarina[1], Audrey M. Neyrinck[1], Patrice D. Cani[1,3], Sandrine P. Claus[4], Nathalie M. Delzenne[1] & Laure B. Bindels[1]*

[1]*Metabolism and Nutrition Research Group, Louvain Drug Research Institute, UCLouvain, Université catholique de Louvain, Brussels, Belgium,* [2]*Nuclear and Electron Spin Technologies Platform (NEST), Louvain Drug Research Institute, UCLouvain, Université catholique de Louvain, Brussels, Belgium,* [3]*Walloon Excellence in Life Sciences and BIOtechnology (WELBIO), Louvain Drug Research Institute, UCLouvain, Université catholique de Louvain, Brussels, Belgium,* [4]*School of Chemistry, Food and Pharmacy, Department of Nutritional Sciences, University of Reading, Reading, UK*

Abstract

Background Cancer cachexia is a multifactorial syndrome characterized by multiple metabolic dysfunctions. Besides the muscle, other organs such as the liver and the gut microbiota may also contribute to this syndrome. Indeed, the gut microbiota, an important regulator of the host metabolism, is altered in the C26 preclinical model of cancer cachexia. Interventions targeting the gut microbiota have shown benefits, but mechanisms underlying the host–microbiota crosstalk in this context are still poorly understood.

Methods To explore this crosstalk, we combined proton nuclear magnetic resonance (^{1}H-NMR) metabolomics in multiple compartments with 16S rDNA sequencing. These analyses were complemented by molecular and biochemical analyses, as well as hepatic transcriptomics.

Results ^{1}H-NMR revealed major changes between control (CT) and cachectic (C26) mice in the four analysed compartments (*i.e*. caecal content, portal vein, liver, and vena cava). More specifically, glucose metabolism pathways in the C26 model were altered with a reduction in glycolysis and gluconeogenesis and an activation of the hexosamine pathway, arguing against the existence of a Cori cycle in this model. In parallel, amino acid uptake by the liver, with an up to four-fold accumulation of nine amino acids (q-value <0.05), was mainly used for acute phase response proteins synthesis rather than to fuel the tricarboxylic acid cycle and gluconeogenesis. We also identified a 35% reduction in hepatic carnitine levels (q-value <0.05) and a lower activation of the phosphatidylcholine pathway as potential contributors to the hepatic steatosis present in this model. Our work also reveals a reduction of different beneficial intestinal bacterial activities in cancer cachexia. We found decreased levels of two short-chain fatty acids, acetate and butyrate (72% and 88% reduction in C26 caecal content; q-value <0.001), and a reduction in aromatic amino acid metabolites, which may contribute to the altered intestinal homeostasis in these mice. A member of the *Ruminococcaceae* family (ASV 2) was identified as the main bacterium responsible for the drop in butyrate. Finally, we report a two-fold intestinal transit acceleration (P-value <0.001) as a key factor shaping the gut microbiota composition and activity in cancer cachexia, which together lead to a faecal loss of proteins and amino acids.

Conclusions Our work highlights new metabolic pathways potentially involved in cancer cachexia and further supports the interest of exploring the gut microbiota composition and activity, as well as intestinal transit, in cancer patients with and without cachexia.

Keywords Cancer cachexia; Liver steatosis; Gut microbiota; Gut transit; Short-chain fatty acids; C26 model; LLC model

Received: 3 July 2020; Revised: 11 December 2020; Accepted: 10 January 2021
**Correspondence to: Laure B. Bindels, Metabolism and Nutrition Research Group, Louvain Drug Research Institute, UCLouvain, Université catholique de Louvain, Avenue E. Mounier, 73, B1.73.11 Brussels, Belgium. Email: laure.bindels@uclouvain.be*

Introduction

Cancer cachexia is a multifactorial syndrome characterized by body weight loss, weakness, muscle atrophy, and fat depletion.[1–3] The observed metabolic alterations are thought to be driven by an extreme inflammatory status resulting from the tumour and the tumour-immune system crosstalk.[1,2] Cachexia affects up to 70% of cancer patients, depending on the cancer type. It worsens prognosis and quality of life and reduces tolerance and response to anticancer treatments. Therefore, cachexia could be the cause of 20% of cancer-related deaths.[1]

Although the muscle is often considered as the key organ in cancer cachexia, other organs may be participating to the pathogenesis of this systemic syndrome.[2,4] The liver is a key organ in metabolism and energy regulation. In cancer cachexia, hepatic alterations are suggested to contribute to the increased energy dissipation. An example of these futile cycles occurring in the liver is the Cori cycle. It refers to the hepatic conversion of tumour-derived lactate to glucose.[2,5] The glucose produced could fuel tumour growth. A major activation of the liver acute phase response (APR) is also observed and was shown to correlate with increased resting energy expenditure in pancreatic cancer patients.[6] Preclinical studies have reported a few changes in liver metabolism such as alterations in mitochondrial function and decreased oxidative phosphorylation,[7] increased hepatic triglyceride levels leading to hepatic steatosis,[8,9] confirming the interest of studying liver metabolism in the cachexia syndrome. Another important regulator of host metabolism and immunity is the gut microbiota.[10–12] Its potential implication in cancer has been investigated for years.[13,14] A common gut microbial signature has been shown in preclinical models of cancer cachexia and nutritional interventions targeting the microbiota impact, in a positive way, cancer progression, morbidity, fat mass loss, and survival of cachectic mice with leukaemia.[15–17]

Even though interventions targeting the gut microbiota have shown benefits, the mechanisms underlying the host–microbiota crosstalk in this context are still poorly understood. To explore this crosstalk, we combined 16S rDNA sequencing, an approach to assess the gut microbiota composition, with proton nuclear magnetic resonance (^{1}H-NMR) metabolomics. ^{1}H-NMR metabolomics is a robust technique to identify small metabolites, including those from glycolysis, tricarboxylic acid (TCA) cycle, and amino acid metabolism, present in biological fluids or tissues extracts.[18] Combining those analyses is of particular interest because bacteria contribute to approximately 70% of faecal and 15% of serum metabolites.[19] The importance of combined *-omics* approaches for studying such relationships has in fact been highlighted by recent works in other (patho)physiological contexts. For instance, Hoyles *et al*. have recently demonstrated the implication of phenylacetic acid, a microbial product of aromatic amino acid metabolism, in triggering steatosis and branched-chain amino acid metabolism by using a *multi-omics* approach.[20] The interest in using *-omics* technologies has also been expressed to help understanding metabolic alterations associated with cancer cachexia.[21,22]

A pioneer metabolomics study of cachexia in the mouse colon carcinoma 26 (C26) model revealed distinct alterations in glucose and lipid metabolism.[23] The same team showed, through a serum metabolomics study, a specific effect of cancer cachexia (C26 model) compared with starvation.[24] More recently, a combined approach using ^{1}H-NMR and mass spectrometry metabolomics in plasma, muscle, and liver extracts of C26 mice has pinpointed different metabolic alterations of cancer-induced and chemotherapy-induced cachexia.[22] Another team showed, in the same model using mass spectrometry metabolomics analyses, that experimental cancer affects muscle and blood metabolomes.[25] They also identified free phenylalanine as a promising biomarker of muscle atrophy and cachexia.

In our study, we did not only apply multi-compartment metabolomics analyses in the C26 model, but we also integrated our data with a hepatic whole transcriptome dataset and with caecal metagenomics. Using such molecular system biology approach, we uncovered new pathways potentially involved in metabolic alterations characteristics of the cachexia syndrome, including changes in gut microbial activity.

Materials and methods

Cell culture

Colon carcinoma 26 (C26) cells were maintained in high-glucose Dulbecco's modified Eagle's medium supplemented with 10% foetal bovine serum (PAA clone, PAA, Austria), 100 μg/mL streptomycin, and 100 IU/mL penicillin (Gibco, Belgium) at 37°C with 5% CO_2.

Mouse experiments

Male CD2F1 mice (6–7 weeks old, Charles River Laboratories, Italy) were housed in individually ventilated cages with a 12 h light/dark cycle and fed with an irradiated chow diet (AO4-10, 2.9 kcal/g, SAFE, France). After an acclimatization period of 7 to 10 days, either a saline solution or C26 cells (1×10^6 cells in 0.1 mL saline) were injected subcutaneously in these 8-week-old animals. All C26-injected mice displayed a tumour mass observable after 7 days. Food intake and body weight were recorded. Eight mice were randomly assigned in each group based on their body weight on the day of cell injection. Ten days after cancer cell injection, mice were fasted for 5 h prior necropsy. Blood samples were harvested following anaesthesia (isoflurane gas, Abbot, Belgium). Tissues were collected,

weighed, and frozen in liquid nitrogen. All of the samples were stored at −80°C until further analyses.

Intestinal transit time was evaluated through a 100 μL gavage of an Evans Blue (50 mg/mL) and microcrystalline cellulose (0.5%) saline solution (NaCl 0.9%), 10 min before mouse anaesthesia.[26] The ratio between the coloured section of the intestine and the total intestinal length (from duodenum to caecum) was calculated. For all NMR metabolomics analyses but one, two independent mouse experiments were used to ensure robustness in our findings. Specific details about each of the mouse experiments presented in this article are reported in the Supporting Information.

For the BaF model, mice were housed in the same environment than the C26 model. Either a saline solution or BaF cells (pro-B lymphocyte cell line transfected with Bcr-Abl, 1×10^6 cells in 0.1 mL saline) were injected into the tail vein of anaesthetized female Balb/c mice (6 weeks old) as previously described.[27]

The experiments were approved by and performed in accordance with the guidelines of the local ethics committee from the Université catholique de Louvain. Housing conditions were as specified by the Belgian Law of 29 May 2013, regarding the protection of laboratory animals (Agreement No. LA1230314).

For the Lewis lung carcinoma (LLC) model, C57Bl/6J mice (local husbandry, Turin, Italy) were kept in specific pathogen-free conditions and housed in individually ventilated cages with a 12 h light/dark cycle and fed with an irradiated standard chow diet. LLC cells were injected in the right bottom flank at 1×10^6 cells in 0.1 mL saline, and mice were necropsied 21 days after cell injection. The experiment was performed in accordance with local and national committees based on Italian Law DL 26/2014.

^{1}H-NMR metabolomics analyses

Sample preparation

Liver samples (n = 32) were prepared according to the methanol/chloroform water procedure described by Beckonert *et al.*[28] Briefly, 100 mg of tissue was mixed with a TissueLyser (Qiagen, Germany) with 1 mL of a cold water–methanol solution (1:1). The mixture was then mixed with chloroform (600 μL) before being centrifuged (15 min, 1000 g, 4°C). The upper polar phase was then evaporated at 37°C under vacuum (CentriVap Labconco) before being diluted into the NMR buffer [H_2O–D_2O (1:1), pH = 7, trimethylsilylpropanoic acid (TSP) 1 mM as standard] and transferred into 5-mm-diameter NMR tubes.

Caecal content (CC) samples (n = 16) were prepared as follows: 35 mg of CC was diluted into 525 μL NMR buffer and homogenized in a TissueLyser. The homogenate was centrifuged (10 min, 13 000 g, 4°C). The supernatant was then transferred into 5-mm-diameter NMR tubes.

Serum samples (n = 32) for both portal vein (PV) and vena cava (VC) were prepared as follows: 40 μL of serum was mixed with 20 μL of NMR buffer (H_2O–D_2O (1:1), pH = 7, TSP 0.1 M). The mixture was then centrifuged (5 min, 12 000 g, 4°C) and transferred into 1.7-mm-diameter NMR tubes.

Data collection

Nuclear magnetic resonance data were acquired on a Bruker Avance 600 MHz NMR spectrometer equipped with a cryoprobe. During acquisition, sample temperature was maintained at 300 K. Spectra were collected with a 1D NOESY pulse sequence for the liver extract samples and with a 1D CPMG pulse sequence for the serum and CC. The 1D NOESY pulse sequence covered 21 ppm. Spectra were digitized in 65 K data points during a 2.6 s acquisition time. The mixing time was set to 10 ms, and the relaxation delay between scans was set to 4 s. The 1D CPMG pulse sequence covered 20 ppm. Spectra were digitized in 65 K data points during a 2.7 s acquisition time. The relaxation delay between scans was set to 4 s. Spectra were acquired using 516 scans for serum samples, 256 scans for CC samples, and 128 scans for liver samples. To confirm metabolite identification, 2D ^{1}H–^{1}H NMR spectra, such as J-RES and TOCSY, as well as ^{1}H–^{13}C HSQC, were acquired for selected samples.

Data processing

The data were processed using MestReNova (v14.1). The spectra were zero filled with a factor of 2, except for liver spectra for which a factor of 4 was used. They were apodized using a 0.3 Hz decaying exponential function and fast Fourier transformed. Automated phase correction and second-order polynomial baseline correction were applied to all samples. All spectra were aligned on the lactate doublet. Spectral quality control was performed, and a few spectra were excluded. Only the region from 0.12 to 10 ppm was conserved. Water signal was removed from all spectra before statistical analyses. Normalization was performed on total peak area. Intelligent bucketing was realized using the MATLAB software (v9.2).[29]

Metabolites were assigned using the Chenomx NMR Suite (v8.43), the Bruker B-BIOREFCODE database (Amix software v3.9.15), the Human Metabolome Database,[30] and additional 2D NMR experiments on selected representative samples. The Chenomx NMR Suite was used to perform a relative quantification of the identified metabolite concentrations. TSP was used as a chemical shift and quantification reference for all spectra. Quantitative fitting of each spectrum was carried out in batch mode, followed by manual adjustment. The mixture of bile acids as well as glycogen was quantified using spectral integration and not with the Chenomx NMR Suite. The peaks used for quantification are given in *Table* S1.

Tissue mRNA analyses

Total RNA was isolated from tissue by TriPure reagent (Roche, Basel, Switzerland). cDNA was prepared by reverse transcription of 1 μg total RNA using the Reverse Transcription System or the Goscript RT Mix OligoDT kit (Promega, Leiden, the Netherlands). Real-time polymerase chain reactions (PCRs) were performed with a QuantStudio Real-Time PCR System and software or a CFX96 TouchTM instrument and software using SYBR Green (Applied Biosystems, Promega, or Eurogentec, Seraing, Belgium) for detection. All samples were run in duplicate in a single 96-well reaction plate, and data were analysed according to the $2^{-\Delta\Delta CT}$ method. The purity of the amplified product was verified by analysing the melt curve performed at the end of amplification. The ribosomal protein L19 (*Rpl19*) and the ribosomal protein L6 (*Rpl6*) genes were chosen as reference genes for all tissues. The primer sequences for the targeted mouse genes are detailed in *Table* S2.

Hepatic whole transcriptome

The hepatic whole transcriptome dataset was previously generated in our lab.[31] Hepatic RNA samples were sequenced after polyA selection using a 2 × 150 paired-end configuration on an Illumina HiSeq 4000 instrument (Genewiz, Germany). Raw sequence data generated from Illumina HiSeq were processed using Illumina's bcl2fastq 2.17 software. Raw fastq files were analysed *in-house* using FastQC, Trimmomatic,[32] STAR,[33] and the R package *GenomicAlignments*.[34] Data were tested for differential expression and normalized using the R package *DESeq2*.[35]

Gut microbiota analyses

Genomic DNA was extracted from the CC (n = 8, CT and C26 groups) using a QIAamp DNA Stool Mini Kit (Qiagen), including a bead-beating step. 16S rDNA sequencing and ensuing bioinformatics and biostatistics analyses [including amplicon sequence variants (ASVs) identification[36]] were performed as previously described.[37] Raw sequences can be found in the SRA database (project ID: PRJNA636939). Full details are provided in the Supporting Information.

Lipid and triglyceride quantification

Triglycerides were measured in the liver tissue after extraction with chloroform–methanol according to the Folch method, as previously described.[38]

Western blot analyses

Liver samples were homogenized and diluted (1/10). Protein concentration was measured using the Lowry method (DC Protein Assay, Bio-Rad, Hercules, CA, USA). Liver protein (40 μg) was separated by 15% SDS-PAGE and transferred to nitrocellulose membrane using the Trans-Blot Turbo Transfer System (Bio-Rad) before blocking in Tris-buffered saline–Tween 20 containing 5% non-fat dry milk (Bio-Rad) for 1 h at room temperature. Membranes were incubated overnight at 4°C with primary antibodies (dilution 1/10 000 in 1% non-fat milk in TBS-T; Cell Signaling Technology, Danvers, MA, USA) detecting β-actin (ab6276; Abcam, Wathan, MA, USA), phospho-AMP-activated protein kinase (AMPK) (Thr 172, 07.681; Millipore, Burlington, MA, USA), and AMPK (Cell Signaling Technology: 2603). After membrane washing, horseradish peroxidase-linked secondary antibodies [Goat Anti-Rabbit IgG (AP 132; Millipore); 1/10 000 in 1% non-fat milk in TBS-T; Cell Signalling Technology] were incubated for 1 h at room temperature. Signals were revealed using the SuperSignal West Pico and Femto Chemiluminescent substrates (Thermo Fisher Scientific, Watham, Massachusetts, USA) and analysed with the ImageQuant TL instrument and software (v.8.1).

Protein and water quantification in faeces

Faeces were homogenized through sonication in phosphate-buffered saline and centrifuged; 1 mL of saturated ammonium sulfate solution was added to the supernatant to precipitate the proteins. After 15 min, the mixture was centrifuged, and the pellet was suspended in 0.5 mL of sodium acetate buffer (50 mM). Protein concentration was then determined using the Pierce method (Pierce™ Prestained Protein MW Marker, Thermo Scientific™). Faeces produced over 24 h were collected and freeze-dried for another 24 h. Water content was determined by weighting samples before and after freeze-drying.

Urea and β-hydroxybutyrate quantification

Urea was quantified in the plasma by spectrophotometry (Urea FS*, DiaSys) according to manufacturer's instructions. β-Hydroxybutyrate was quantified in the plasma by spectrophotometry (β-hydroxybutyrate 21 FS*, DiaSys) according to the manufacturer's instructions. For liver samples, a similar extraction than for ^{1}H-NMR measurements was performed. Briefly, 100 mg of tissue was mixed with a TissueLyser (Qiagen) with 1 mL of a cold water–methanol solution (1:1). The mixture was then mixed with chloroform (600 μL) before being centrifuged (15 min, 1000 g, 4°C). The upper polar phase was then evaporated at 37°C under vacuum (CentriVap

Labconco) before being diluted into 200 μL of water; 12 μL of this extract was then used for further quantification by spectrophotometry.

Statistical analyses

Biochemical and molecular analyses

Outliers were removed using the Grubbs test. Normality was assessed using d'Agostino and Pearson omnibus normality test. If normality was not respected in one group, the non-parametric Mann–Whitney *U* test was used. In pair-feeding experiment, paired comparisons were performed (CT vs. C26 and PF-CT vs. PF-C26). Fisher's exact test was used to check for variance equality between groups. Student's *t*-test was used when variances were not statistically different. In case of variance inequality, Welch's *t*-test was used. Statistical analyses were performed using GraphPad Prism 5.0 and R.[39] $P < 0.05$ was considered statistically significant.

Gut microbiota data analyses

Significantly affected ASVs (with an average relative abundance superior to 0.1% in at least one group), phyla, families, and pathways were identified using a Mann–Whitney *U* test in R because normality was not respected for every ASV/phylum/family/pathway. The *P*-value was adjusted to control the false discovery rate for multiple testing according to the Benjamini and Hochberg procedure.[40]

Metabolomics data analyses

The matrix resulting from the intelligent bucketing was imported in R. A principal component analysis (PCA) with scaling to unit variance was performed using the *pca* function of the *mixOmics* package.[41] Overlay of CT and C26 average spectra was generated using an *in-house* script using the *plotrix*,[42] *colorRamps*,[43] and *autoimage*[44] R packages.

The table of metabolite concentration was also analysed in R. A PCA with scaling to unit variance was performed. Significantly affected metabolites were identified by a Mann–Whitney *U* test. The *P*-value was adjusted to control for the false discovery rate. Changes were visualized for each metabolite using the *ggplot* function in the *tidyverse* package.[45] The *bubbleplot* was generated using an *in-house* script including the *tidyverse* R package.

Integration analyses

Amplicon sequence variants with an average relative abundance superior to 0.1% in at least one group were selected for further integration analyses. A partial least squares analysis in canonical mode was used to maximize the correlations between the gut microbiota (after centred log-ratio transformation) and the CC metabolomics datasets.[46] This function is implemented in the *mixOmics* package. Results were visualized through a clustered image map.[47]

Results and discussion

^{1}H-NMR metabolomics reveals major changes in the caecal, hepatic, portal, and systemic blood metabolomes of cachectic mice

The presence of cachexia in C26 mice was confirmed based on a reduction in body weight, food intake, and muscle mass in these mice (*Figure* S1). Liver, CC, portal blood, and systemic blood were harvested, and ^{1}H-NMR spectra were acquired from these samples. Spectra were first analysed using multivariate statistical tools. PCA performed both on the spectral intelligent bucketing (*Figure* S2a–S2d) and on the metabolite relative concentration tables (*Figure* 1A–1D) highlighted a clear distinction between CT and C26 samples in the four compartments. This separation, occurring mainly along the first principal component (PC1), shows that cachexia is the major source of variation in these datasets. This clear distinction between CT and C26 metabolomics profiles was also visible on the superposition of each group average spectrum (*Figure* S2e–S2h). A maximum number of metabolites were identified with certainty in the four compartments (*Table* S1). A relative quantification was applied, and *Figure* 2 depicts the observed fold changes for each metabolite in the four compartments. A descriptive table presenting the numeric fold changes and statistics is available (*Table* S3). At first glance, most identified metabolites seemed to be increased in cachectic liver and CC while decreased in the portal and systemic circulation (*Figures* 1E–1H and 2). Metabolites were manually grouped into five categories to facilitate interpretation and discussion: metabolites related to glucose metabolism, energy status, amino acids, lipid metabolism, and gut microbiota.

Cachectic mice display altered glucose metabolism pathways and present an energy deficiency

Changes in identified metabolites related to glucose metabolism in the liver and portal and systemic circulation suggest a general depletion of glucose related metabolites. *Figure* 3A summarizes the observed changes in the liver. Glycogen, glucose, and lactate were decreased, whereas UDP-glucose was increased in C26 liver. The other identified metabolites were unchanged between CT and C26 mice. In C26 PV and VC, glucose, lactate, pyruvate, and citrate were decreased. These changes mainly confirm the results of a previous metabolomics study in the serum and liver of C26 mice.[22] We also found a decrease of glucose storage in the form of glycogen as well as a decrease of glucose itself. This can be explained by the starvation status and the reduced food intake of these mice (*Figure* S1a and S1b). Identified TCA cycle intermediates were unchanged.

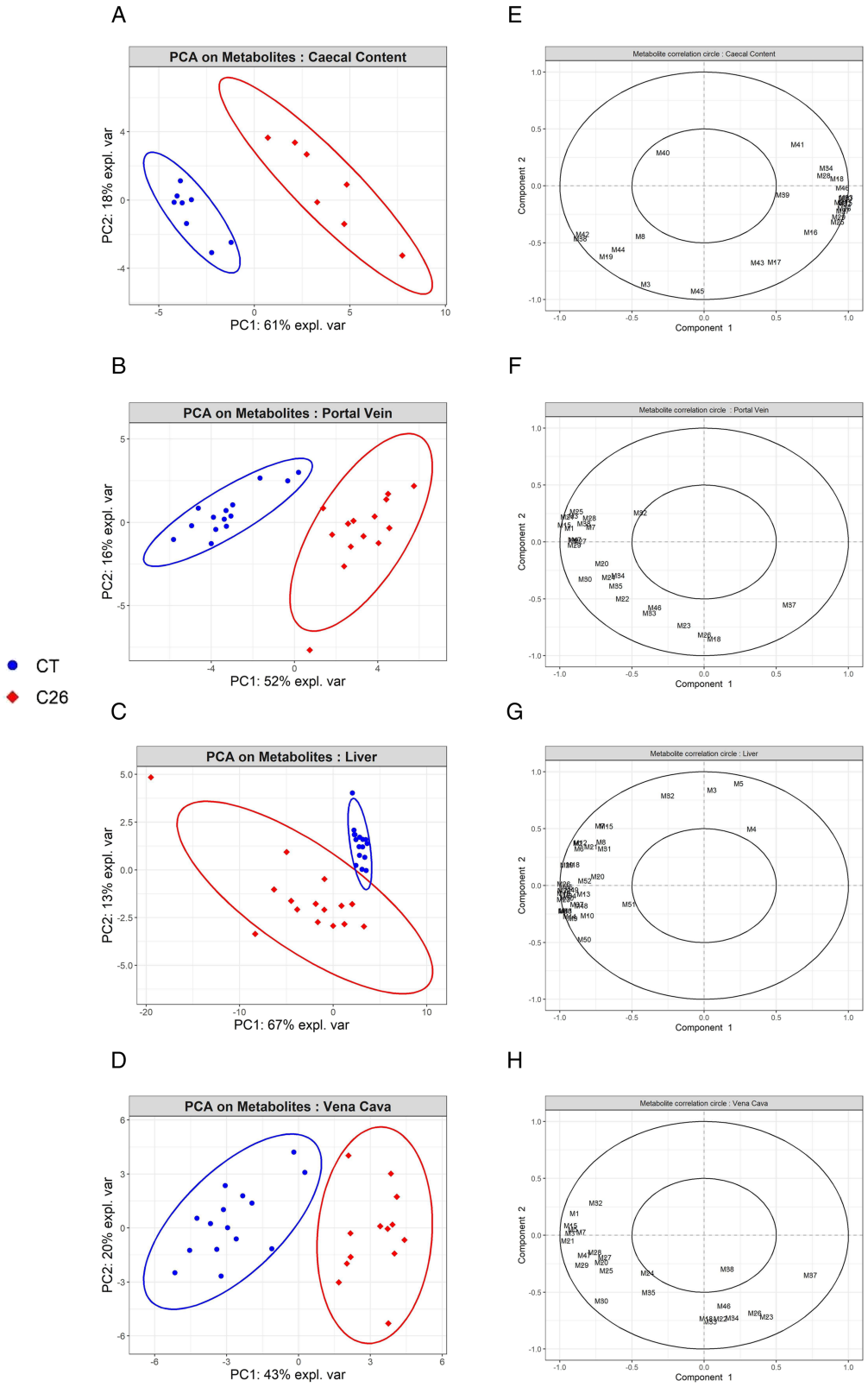

Figure 1 Principal component analyses (PCAs) on identified metabolites in control (CT) and cachectic (C26) mice in the four compartments. (A–D) Normalized PCA realized on the metabolite relative concentration matrices in the caecal content (CC), portal vein (PV), liver, and vena cava (VC) in CT (blue dots) and C26 (red diamonds) mice. (E–H) Correlation circle plots of the PCA analyses in the CC, PV, liver, and VC. The identity of the metabolites can be found in *Table* S3. Caecal content: n = 8 per group. Portal vein, liver, and vena cava: n = 16 per group.

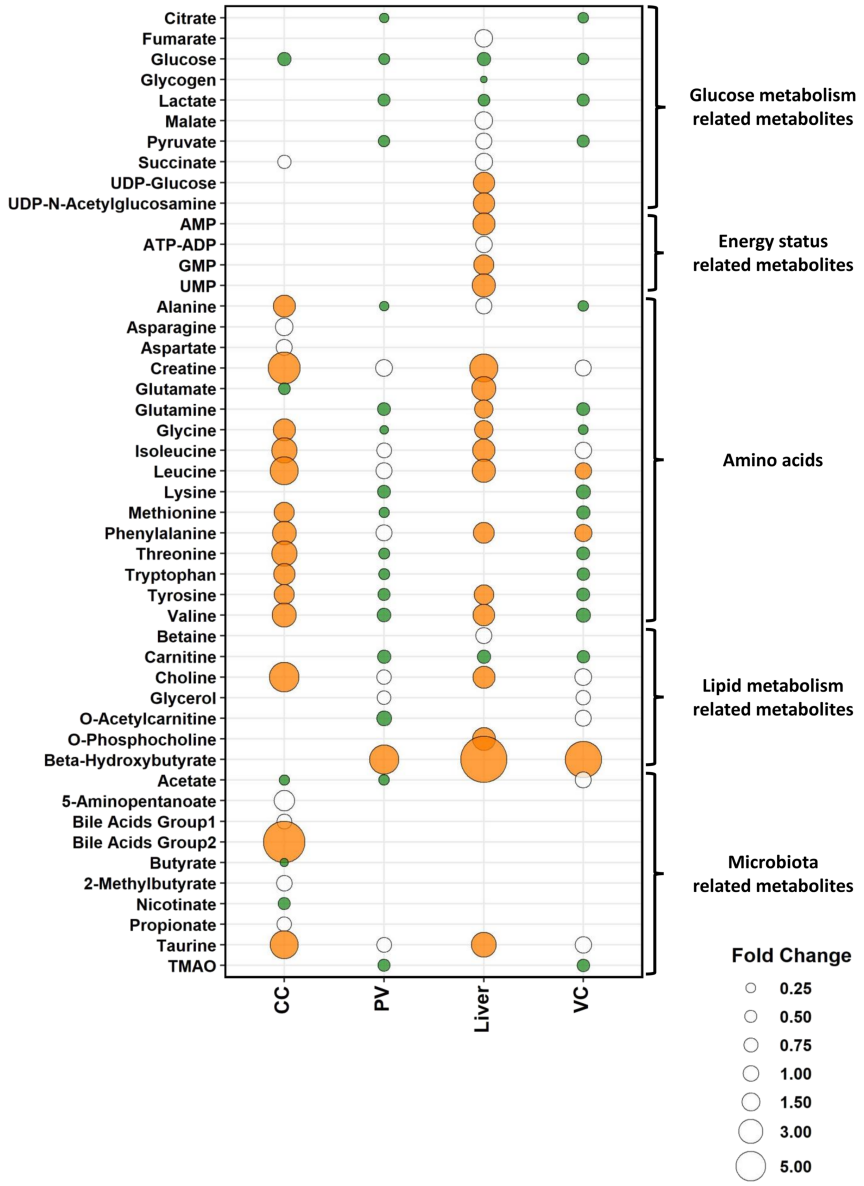

Figure 2 Bubbleplot presenting metabolite concentration changes in the four compartments. Metabolites are grouped into five categories corresponding to the pathways they are related to. Bubble size depicts concentration fold change. Coloured bubbles correspond to significantly changed metabolites in cachectic (C26) mice. Orange and green are used respectively for increased and decreased metabolite concentrations. Caecal content (CC): n = 8 per group. Portal vein (PV), liver, and vena cava (CV): n = 16 per group.

These data were analysed in light of the results from a hepatic whole transcriptome analysis performed on a similar independent mouse experiment. The expression of the glucokinase (*Gk*), a key glycolysis enzyme regulated at the transcription level, was decreased in C26 mice reflecting a reduction in hepatic glycolysis (*Figure* 3B). We cannot exclude that the reduction in glycogen and in hepatic and systemic glucose could also be the result of an increased glucose demand and consumption by extrahepatic tissues (*i.e.* skeletal muscles and tumour). More surprisingly, two gluconeogenic enzymes *Pck1* and *G6pc*, the phosphoenolpyruvate kinase and the glucose-6-phosphatase, also regulated at the transcription level, were respectively unchanged and decreased in C26 mice (*Figure* 3B). The G6Pase is also catalyzing the final step of the glycogenolysis. Factors explaining the reduced expression of the catalytic subunit *G6pc* include a reduction in hepatic glucose and high plasma IL-6 levels.[48] The absence of gluconeogenesis activation in the liver of cachectic mice goes against the Cori cycle hypothesis commonly mentioned as a futile cycle taking place in cancer cachexia.[2] The decrease in lactate, both in systemic circulation and in the liver, probably reflects a decreased muscular and hepatic glycolysis rather than an increased hepatic lactate–glucose conversion through gluconeogenesis.

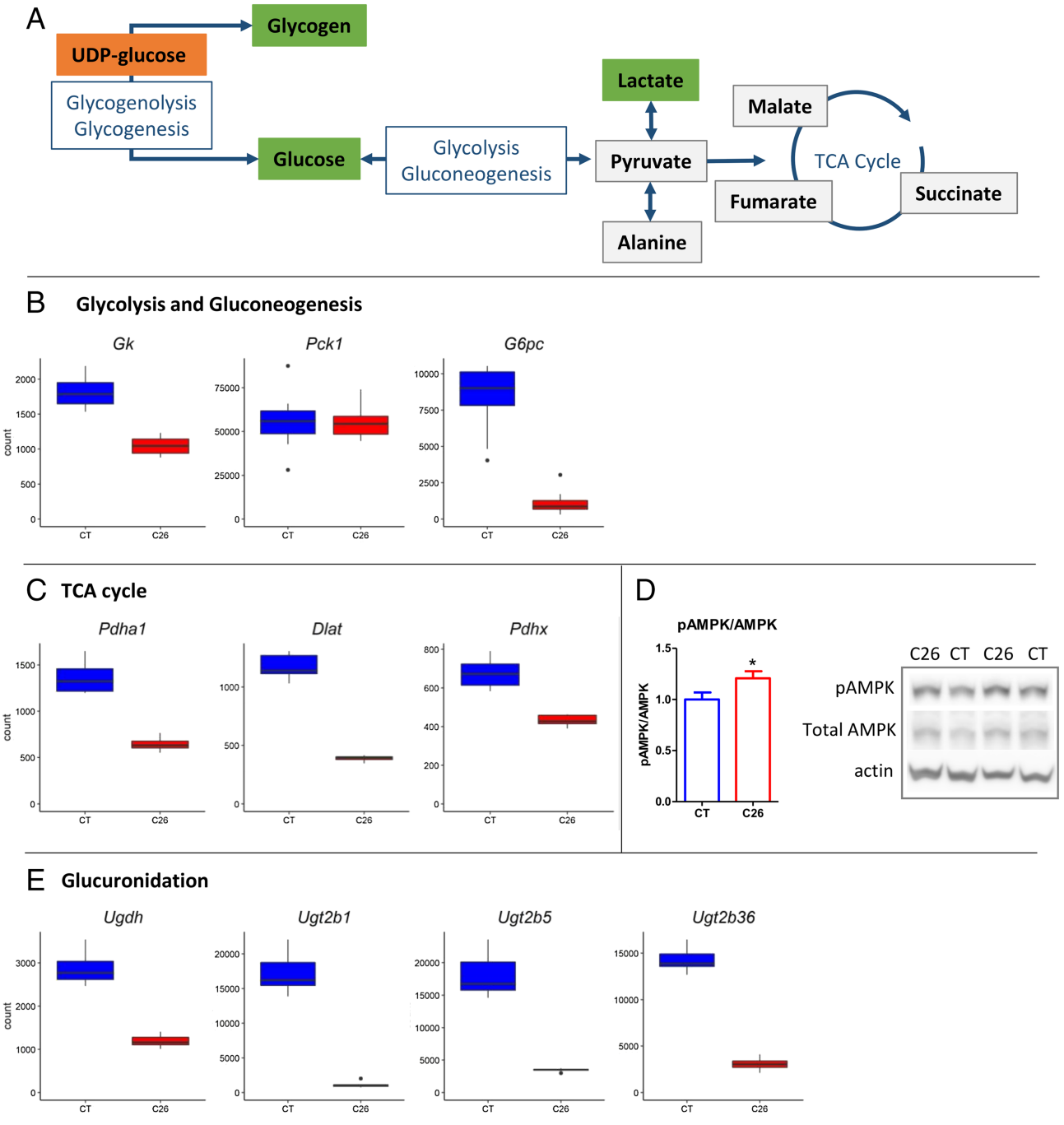

Figure 3 Glucose metabolism is decreased in cachectic mice (C26) presenting an energy deficiency in the liver. (A) Schematic view of glucose metabolism in the liver of control (CT) and C26 mice. Metabolites in orange are significantly increased in C26 mice; metabolites in green are significantly decreased in C26 mice; and metabolites in grey are identified but unchanged between groups. (B, C, E) RNAseq data expressed in counts (n = 8 per group). (B) *Gk* [$\log_2$ fold change (L2FC): −0.80***] coding for glucokinase is a key glycolysis enzyme. *Pck1* (ns) and *G6pc* (L2FC: −2.86***) coding respectively for the phosphoenolpyruvate kinase and glucose-6-phosphatase catalytic subunit are two key gluconeogenic enzymes. (C) Pyruvate dehydrogenase complex [*Pdha1* (L2FC: −1.07***), *Dlat* (L2FC: −1.59***), and *Pdhx* (L2FC: −0.65***)] is the complex responsible for pyruvate entrance in the TCA cycle. (D) Phosphorylation levels of the AMP-activated protein kinase and representative western blots (n = 16 per group). (E) *Ugdh* (L2FC: −1.28***) is coding for UDP-glucose-6-dehydrogenase. *Ugt2b1* (L2FC: −3.95***), *Ugt2b5* (L2FC: −2.37***), and *Ugt2b36* (L2FC: −2.22***) are coding for the three main UDP-glucuronosyltransferases in mice. *P-value <0.05; ***q-value <0.001.

DOI: 10.1002/jcsm.12684

The expression of the enzymes forming the pyruvate dehydrogenase complex: *Pdha1*, *Dlat*, and *Pdhx*, was reduced (*Figure* 3C). This complex is responsible for pyruvate conversion into acetyl-CoA and subsequent entry in the TCA cycle. The decreased expression of these enzymes suggests a reduced entry of glucose derived pyruvate in the TCA cycle. A recent liver proteomics study in the C26 model also showed a decrease in PDHX.[49] In all, this reflects the decreased oxidative pathways providing ATP in the liver of C26 mice, which is consistent with previous studies reporting a decreased efficiency of oxidative phosphorylation in liver mitochondria in cancer cachexia.[7] The increased levels of AMP, GMP, and UMP in the liver of C26 mice (*Figure* 2) and the activation of the AMPK (*Figure* 3D) further support this idea.

Glucuronidation is decreased while the hexosamine pathway is activated in cachectic mice

We also observed hepatic accumulation of UDP-glucose and UDP-*N*-acetylglucosamine (*Figure* 2). UDP-glucose is the precursor of glucuronic acid, the cofactor needed for glucuronidation. Its accumulation, in parallel with the lower expression of *Ugdh* (*Figure* 3E), encoding the UDP-glucose-6-dehydrogenase, a key enzyme regulated at the mRNA level,[50] suggests a decreased glucuronidation. This hypothesis is further strengthened by the lower mRNA levels of *Ugt2b5*, *Ugt2b1*, and *Ugt2b36*, coding for the main murine UDP-glucuronosyltransferases (*Figure* 3E).[51]

The increase in UDP-*N*-acetylglucosamine can be explained by the lower glycolysis rate and the up-regulation of the hexosamine synthesis pathway (*Figures* 2 and S3a). The increase in the latter most probably results from endoplasmic reticulum stress, which involvement in cancer cachexia has already been suggested, although the exact mechanisms are still unknown.[52,53] Indeed, the spliced X-box binding protein 1 (*Xbp1s*), the most conserved signal transducer of the unfolded protein response, was increased in C26 liver (*Figure* S3b) and has been shown to activate the hexosamine pathway through the induction of *Gfpt1*.[54] The latter encodes the rate-limiting enzyme of the hexosamine pathway and is regulated at the transcription level.[55] In accordance with our hypothesis, *Gfpt1* expression was significantly increased in C26 liver (*Figure* S3a). UDP-*N*-acetylglucosamine plays an important role in the reversible post-translational modification of proteins (*O*-GlcNAcylation), which can impact signal transduction.[55] Interestingly, an increase in GlycA, an aggregate signal of *N*-acetyl glycan groups attached to APR proteins, is considered as a novel biomarker of systemic inflammation[56] and has been observed in a previous serum metabolomics study in the C26 model.[22] This observation further supports the idea of an activation of the hexosamine pathway by the UPR, leading to increased *O*-GlcNAcylation and possibly thereby influencing signal transduction.

Amino acids are captured by the liver of cachectic mice mainly for acute phase response protein synthesis

Almost all identified amino acids present in the liver were increased in C26 mice, whereas they were mostly diminished in the portal and systemic circulation (*Figure* 2). These essential and non-essential amino acids are of various structures and uses: branched-chain amino acids, aromatic amino acids, charged amino acids, and ketogenic and glucogenic amino acids. Significant reduction in the plasma levels of branched chain amino acids has already been reported in cachectic preclinical models.[22] Noticeably, phenylalanine, which serum concentration was recently proposed as a biomarker for cancer cachexia,[25] was increased in systemic circulation of C26 mice. The increase in amino acids observed in the liver results from an important uptake of amino acids, mostly coming from muscle proteolysis, as previously reported.[2,57] Indeed, as shown in *Table* 1, the transcription of a large number of hepatic amino acid transporters is up-regulated. This occurs independently of the preferred transported substrate(s).

Amino acid uptake by the liver is commonly seen as fuelling hepatic gluconeogenesis.[2,58] However, as mentioned earlier, this does not seem to be the case in the C26 model. The decreased expression of two key gluconeogenic enzymes, that is, *Pck1* and *G6pc* (*Figure* 3C), of the alanine aminotransferase (*Gpt*, L2FC: −0.52, *q*-value <0.001; *Gpt2*, L2FC: −0.69,

Table 1 Most liver AA transporters are increased at the mRNA level in cachectic mice (C26)

Gene	AA transporter	Predominant substrate(s)	Log_2 FC
Slc1a2	EAAT2/GLT1	L-Glu and D/L-Asp	−0.79
Slc3a1	rBAT	Neutral and basic AAs	4.02
Slc3a2	CD98hc/4F2hc	L-type AAs	0.70
Slc6a9	GlyT1	L-Gly	0.63
Slc7a2	CAT-2	CAAs (L-Arg)	−0.60
Slc7a4	CAT4	CAAs	−0.99
Slc7a5	LAT1	LNAAs	2.06
Slc7a6	y+LAT2	CAAs and LNAAs	1.42
Slc7a7	y+LAT1	CAAs and NAAs	1.76
Slc7a8	LAT2	LNAAs	1.23
Slc7a11	xCT	L-Glu and L-Cys	1.33
Slc15a3	PHT2	L-His	0.79
Slc25a12	AGC-1/Aralar1	L-Glu and D/L-Asp	0.60
Slc25a13	AGC-2/Aralar2	L-Asp and L-Glu	−1.05
Slc25a15	ORNT1/ORC1	L-Om and L-Cit	0.75
Slc36a1	PAT1	Small AAs and GABA	0.44
Slc36a4	PAT4	L-Pro, L-Trp, and L-Ala	0.89
Slc38a1	SNAT1	L-Gln	0.90
Slc38a2	SNAT2	L-Gln	0.88
Slc38a4	SNAT4	L-Gln and L-Arg	−1.10
Slc43a1	LAT3	BCAAs	2.08

AA, amino acid; BCAAs, branched chain amino acids; CAAs, cationic amino acids; LNAAs, large neutral amino acids.
Selected AA transporters from RNAseq data are presented with the log_2 fold change (FC) between C26 and control (CT) mice (n = 8 per group). Predominant substrates are presented according to Kandasamy *et al.*[100] classification. All changes are significant with a *q*-value <0.01.

q-value <0.001), of a key enzyme involved in the production of urea (*Cps1*, L2FC: −1.31, *q*-value <0.001), and of systemic urea levels (CT: 38.56 ± 2.04 mg/dL vs. C26: 27.52 ± 2.85 mg/dL, *P*-value <0.01) argues against the use of amino acids to fuel gluconeogenesis as well as the TCA cycle. In this model, imported amino acids seem to be mainly used for APR protein synthesis. Indeed, we observed a huge increase in the expression of *Apcs*, *Saa1*, and *Saa2* expression, three main murine positive APR protein-coding genes,[59] and a decrease of *Alb* (albumin), the main negative APR protein-coding transcript (*Figure* 4).

The important increase in positive APR proteins has been observed in both clinical and preclinical models of cachexia.[2] Although the use of amino acids for gluconeogenesis in the liver of cachectic individuals is generally mentioned, a study performed in cachectic rats similarly observed an up-regulation of APR protein synthesis at the expense of glucose production.[60] They showed that despite an increase in liver uptake of essential and glucogenic amino acids, glucose and urea production remained unchanged. They concluded that the liver was, in this context, an efficient nitrogen-sparing and active protein-synthesizing organ. Similarly, the increase in protein synthesis was reported to be targeted towards export proteins rather than structural proteins in cachectic patients with colon cancer.[61] To balance the increased protein synthesis, the liver can spare nitrogen through a reduction of structural protein turnover.[62]

In the C26 model, a functional test confirmed an increased hepatic protein synthesis.[63] In addition, we observed a reduction in the expression of *Atg7* (L2FC: −0.53, *q*-value <0.001), a key regulator of autophagy,[64] and *Smurf1* (L2FC: −0.42, *q*-value <0.001), an important E3 ubiquitin protein ligase in the liver,[65] suggesting a reduction in protein degradation for nitrogen sparing. *Atg7* was also decreased in another preclinical model of cachexia (LLC model) in which the authors reported a decrease in autophagy machinery with cancer progression.[66] This might be surprising considering that the hepatic level of autophagic function is significantly increased in response to starvation. However, amino acid levels, especially leucine and glutamine, can exert a suppressive effect on autophagy when their levels reach 2–4 times than usual ones.[64,67] The important increase of these two amino acids in C26 liver (*Figure* 2 and *Table* S3) could explain and support the reduction in liver protein breakdown despite the starvation status. Our observations, combined with others,[66] suggest that these aberrations in autophagy might influence hepatic function in cancer cachexia and deserve further investigations.

Changes in carnitine and choline metabolism may participate in the hepatic steatosis observed in cachexia

Carnitine, an amino acid derivative essential for fatty acid catabolism, was significantly decreased in the serum and liver of C26 mice (*Figure* 2). Such alterations in serum carnitine levels have already been reported in cancer patients with cachexia and in preclinical models of cancer cachexia.[68,69] The hepatic carnitine drop reflects a reduction in hepatic mitochondrial β-oxidation further participating to the energy deficiency status. The lower expression of the enzymes responsible for the first and last steps of mitochondrial β-oxidation, respectively, *Acadm* (L2FC: −0.51, *q*-value <0.001) and *Acaa2* (L2FC: −1.22, *q*-value <0.001), further supports this idea. Yet the expression levels of *Ppargc1a*, a transcriptional coactivator regulating, among others, the genes involved in mitochondrial fatty acid oxidation, and *Cpt1a*, responsible for acyl mitochondrial entry, were unchanged. Changes in CPT1 activity have already been mentioned in preclinical cachectic models despite none or negligible changes at the mRNA level.[69,70] Studies also reported that carnitine supplementation restored CPT1 activity in tumour-bearing mice and rats, which led to improvements in the cancer cachexia syndrome and a reduction in hepatic steatosis in these animals.[69,71,72]

Depending on mammalian diets, exogenous carnitine intake and endogenous carnitine biosynthesis vary.[73] Mice

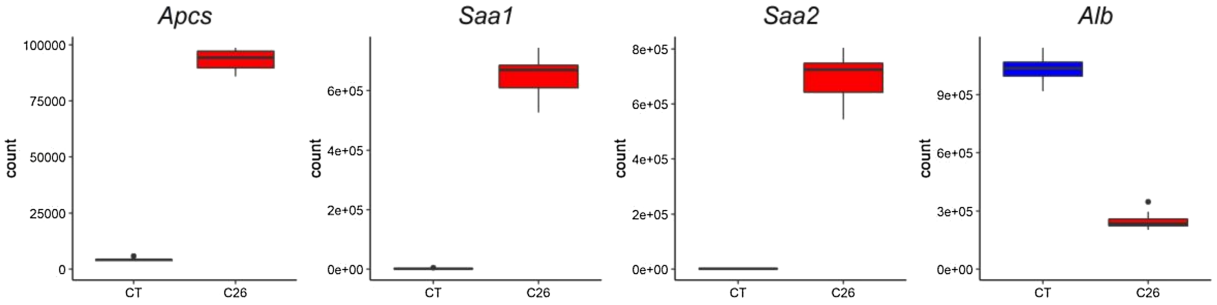

Figure 4 The expression of acute phase response (APR) proteins is increased in the liver of cachectic mice (C26). RNAseq data expressed in counts (*n* = 8 per group). *Apcs* [$\log_2$ fold change (L2FC): 4.45***], *Saa1* (L2FC: 8.38***), and *Saa2* (L2FC: 8.96***) are coding for three major murine APR proteins, which are respectively the serum amyloid P-component, the serum amyloid A1, and the serum amyloid A2. *Alb* (L2FC: −2.04***) codes for albumin. ****q*-value <0.001.

receiving classic rodent diets synthesize carnitine endogenously from lysine and methionine. In our experiment, the carnitine biosynthesis pathway was decreased, fitting the decreased hepatic carnitine concentration (*Figure* 5A). Indeed, the expressions of all enzymes, including the key and rate-limiting enzyme *Bbox1* (γ-butyrobetaine hydroxylase 1),

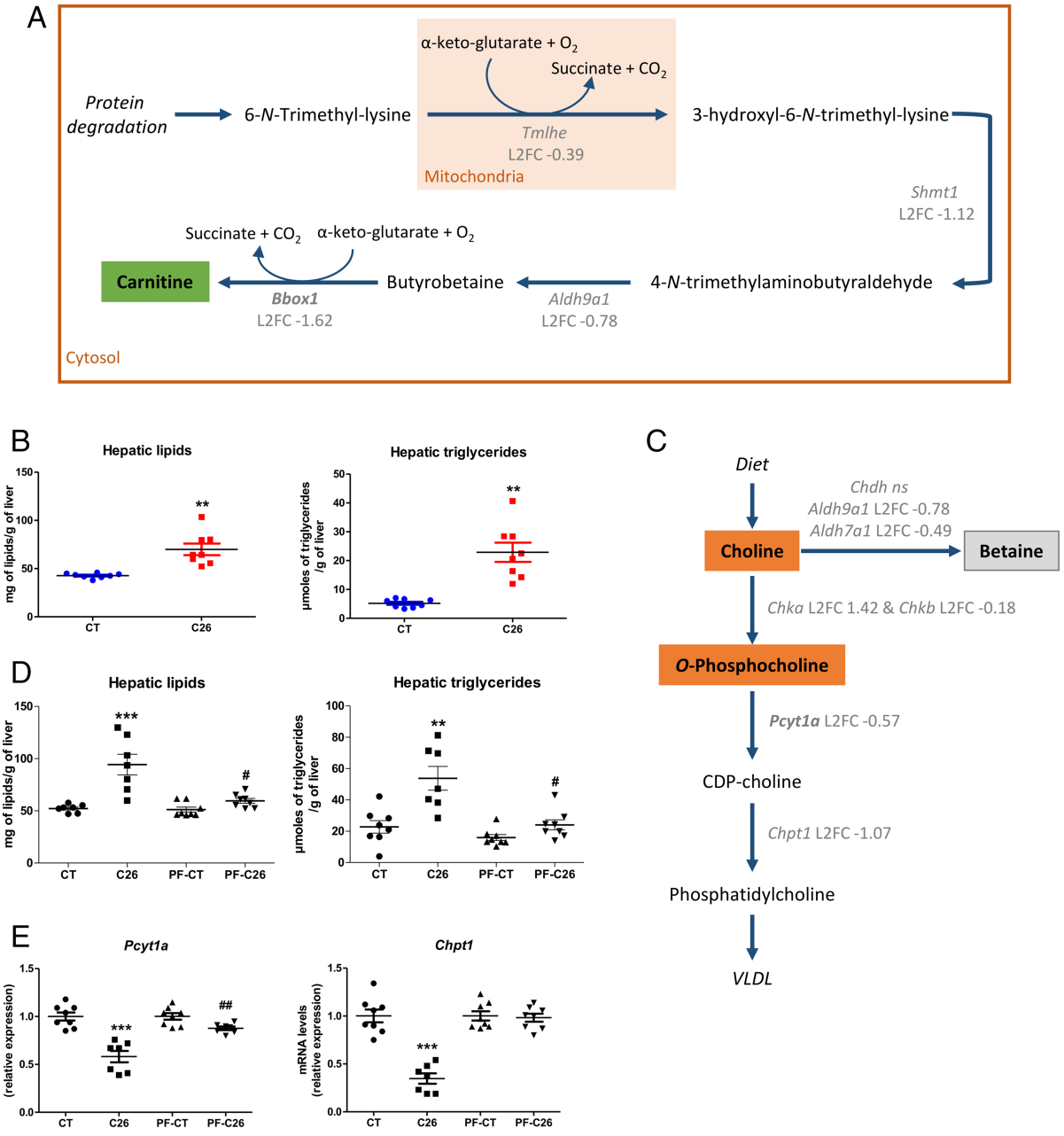

Figure 5 Cachectic (C26) liver displays an increase in hepatic lipids and triglycerides, which is not due to reduced food intake. The hepatic steatosis could be explained by a reduction in carnitine and carnitine biosynthesis, as well as a decreased VLDL excretion. (A) Schematic view of carnitine biosynthesis in the liver of control (CT) and C26 mice. The metabolite in green is significantly decreased in C26 mice. The significant (q-value <0.001) $\log_2$ fold change (L2FC) of the expression of the implicated enzymes in the pathway is shown including *Bbox1* coding for γ-butyrobetaine hydroxylase 1, the rate-limiting enzyme of the pathway. (B) Hepatic lipids and triglycerides in CT and C26 mice (n = 8 per group). (C) Schematic view of choline metabolism and phosphatidylcholine synthesis, a key component of VLDL, in the liver of CT and C26 mice. Metabolites in orange are significantly increased in C26 mice; the metabolite in grey is identified but unchanged between groups. The L2FC of the expression of the implicated enzymes in the pathway is shown including *Pcyt1a* coding for phosphocholine citidyltransferase A, the rate-limiting enzyme. Except for *Chdh*, all changes are significant (q-value <0.01). (D) Hepatic lipids and triglycerides in the pair-feeding experiment (n = 7–8 per group). (E) Expression level of two key enzymes, *Pcyt1a* and *Chpt1*, of choline to phosphatidylcholine transformation in the pair-feeding experiment (n = 7–8 per group). *Comparison between CT and C26 groups; #Comparison between PF-CT and PF-C26 groups.**P-value <0.01; ***P-value <0.001; #P-value <0.05; and ##P-value <0.01.

DOI: 10.1002/jcsm.12684

were significantly decreased. We thus concluded that reduced carnitine levels, likely ensuing from a reduced biosynthesis, may contribute to the hepatic steatosis found in these mice (*Figure* 5B) by limiting mitochondrial β-oxidation.

Our metabolomics analysis pinpointed another pathway that may contribute to hepatic steatosis, mainly the phosphatidylcholine pathway. The levels of choline and *O*-phosphocholine were increased, while the phosphatidylcholine biosynthesis appeared to be reduced in the liver of cachectic mice (*Figures* 2 and 5c). Indeed, we found lower expression of the phosphatidylcholine biosynthetic enzymes, especially *Pcyt1a*, the limiting one. Another pathway leads to phosphatidylcholine synthesis in the liver, with *Pemt* as a key enzyme,[74] and was also decreased in C26 mice (*Pemt*, L2FC: −0.42, *q*-value <0.001). Because phosphatidylcholine enters in the composition of VLDL, lower biosynthesis could affect triglyceride export through VLDL and thereby contribute to the accumulation of triglycerides observed in C26 mice (*Figure* 5B). In accordance with our hypothesis, a previous study documented a reduction in hepatic VLDL secretion in the C26 model.[9]

Prolonged fasting and undernutrition were previously associated with hepatic steatosis.[75] To evaluate whether the reduced food intake observed in the late stage of the disease contributes to the steatosis found in cachectic mice, an independent experiment including pair-fed animals was performed where two groups of healthy mice were pair-fed either to the CT group or to the C26 group. The increase in hepatic lipids and triglycerides in healthy mice enduring food restriction (PF-C26) was much more modest than the one observed in C26 mice (*Figure* 5D). Coherently, the pair-feeding experiment did not recapitulate the reduction in the expression of *Pcyt1a* and *Chpt1*, the two enzymes responsible for the conversion of *O*-phosphocholine into phosphatidylcholine (*Figure* 5E). This experiment establishes that anorexia does not drive hepatic steatosis and the reduction in the phosphatidylcholine pathway.

Altogether, we concluded that a deficit in carnitine and a reduced transformation of choline and *O*-phosphocholine in phosphatidylcholine may contribute to the hepatic steatosis found in C26 mice.

Kidney ketogenesis is substantially increased in cachectic mice and counterbalances hepatic ketogenesis deficiency

The ketone body β-hydroxybutyrate was substantially increased in the liver as well as in the portal and systemic circulation of C26 mice (*Figure* 2). Considering the decreased food intake in cachectic mice, these changes could be expected. However, other works have reported a reduced ketogenic response in cachectic mice compared with healthy food-restricted or starved mice.[76,77] Consistent with the latter observations, we noticed a reduced hepatic expression of *Ppara* (L2FC: −1.67, *q*-value <0.001), a transcription factor regulating ketogenesis in the liver, and *Hmgcs2* (L2FC: −0.89, *q*-value <0.001), a target of *Ppara* and the ketogenesis rate-limiting enzyme. According to Flint *et al*., the important inflammation observed in cancer cachexia and the subsequent increase in IL-6 reduce PPARα activation and ketogenesis.[76] Changes in hepatic fatty acid metabolism, with a decreased β-oxidation, and a potential alteration in autophagy could also participate to a reduced hepatic ketogenic response in C26 mice.[66,78] The alteration in the ketogenic response in C26 mice was confirmed by the measurement of β-hydroxybutyrate and *Hmgcs2* in the pair-feeding experiment. Indeed, we observed similar increase in β-hydroxybutyrate levels in the liver and systemic circulation of food-restricted animals (PF-C26) (*Figure* S4a and S4b), which could, in this case, be explained by hepatic ketogenesis (*Figure* S4c). The contradiction between the metabolomics and transcriptomic results, namely, increased levels of β-hydroxybutyrate and reduction in ketogenesis transcripts, led us to explore alternative pathways for ketone body production. Renal ketogenesis is also possible, especially during starvation.[79] *Hmgcs2* in the kidney of C26 mice was increased by 14-fold (*Figure* S4d). This result provides an explanation for the increased β-hydroxybutyrate levels observed in C26 mice.

Similar hepatic alterations are observed in the Lewis lung carcinoma model

To evaluate the relevance of our findings, we investigated whether similar hepatic alterations were found in another model of cancer cachexia, the LLC model. Similar changes were observed regarding the expression of *G6pc*, whereas, as in C26 mice, no significant change in *Pck1* expression was identified (*Figure* S5a) suggesting a reduction in gluconeogenesis in this model too. We observed a significant increase in the expression of hepatic amino acid transporters (*Figure* S5b). Together with the more than five-fold increase in the major murine positive APR in those mice (*Figure* S5c), those results suggest an important amino acid uptake by the liver and further use for APR protein synthesis. As for the C26 model, reduction in the expression of *Cps1* (*Figure* S5d) goes against the potential use of AA in fuelling the TCA cycle. Despite the absence of hepatic steatosis, alterations related to lipid metabolism were observed, confirming Rosa-Caldwell's work.[66] We indeed noticed a reduction in the expression of *Bbox1*, *Pcyt1a*, and *Chpt1* (*Figure* S5e and S5f), which reflect a reduction in carnitine and phosphatidylcholine synthesis. Finally, although *Hmgcs2* expression tended to be reduced (30% reduction, *P-value* = 0.13), we observed an increase in hepatic β-hydroxybutyrate levels in LLC mice

(*Figure* S5g). Altogether, these results extend our findings to another preclinical model of cancer cachexia.

Several gut microbial activities are decreased in cancer cachexia

The composition of the gut microbiota was altered in C26 mice as shown by two different β-diversity indexes (*Figure* S6a and S6b). The observed changes, mainly a decrease in the Firmicutes phylum and an increase in the Proteobacteria phylum, confirm our previous reports (*Figure* S6c).[15,80] To identify the bacteria responsible for the production of specific metabolites, we performed correlations between metabolites and bacterial ASVs (which refer to inferred individual DNA sequences of the 16S gene[81]) using a canonical partial least squares regression. Canonical partial least squares regression is a method particularly recommended to maximize the correlation between two datasets when the number of variables outnumbers the number of samples. It revealed some strong correlations between specific couples of ASVs and metabolites (*Figure* 6) from which we have targeted the strongest ones for further investigations. The ASV identification is indicated in *Table* S5.

Acetate and butyrate, two short-chain fatty acids, are reduced in cachectic mice

Short-chain fatty acids (SCFAs) are produced mainly through the fermentation of complex carbohydrates by the gut microbiota and are linked to various host health conditions.[82] We

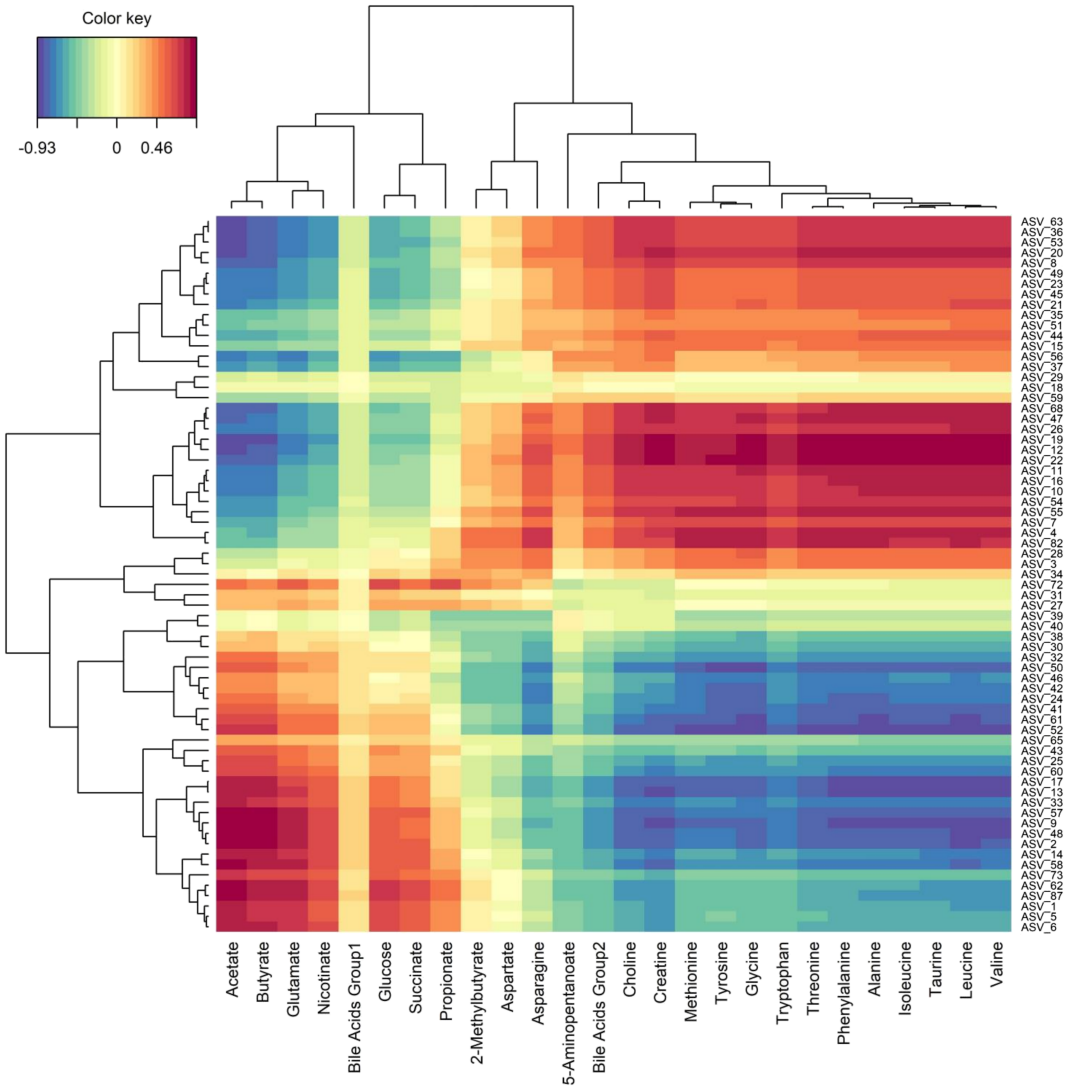

Figure 6 Canonical partial least squares analysis (cPLS) reveals strong correlations between amplicon sequence variants (ASVs) and metabolites in mouse caecal content. Correlations are shown according to a colour gradient going from blue for negative to red for positive correlations. All identified metabolites from the metabolomics analysis performed in the caecal content are in abscissa, and all ASVs (with an average relative abundance superior to 0.1% in at least one group), resulting from 16S rDNA sequencing analysis, are in ordinate. *n* = 8 per group.

show that acetate and butyrate, two SCFAs, were decreased in the CC of cachectic mice, whereas propionate and 2-methylbutyrate remained unchanged (*Figure* 2). Succinate was decreased by 34% (q-value = 0.051). SCFAs are known, among others, to impact colonocyte energy status, gut peptide synthesis, glycaemic response, blood and hepatic lipid content, satiety, and systemic inflammation.[83] As cross-feeding between bacteria occurs mainly from acetate to butyrate,[84] such cross-feeding may justify the concomitant decrease of these two metabolites. The decrease in butyrate and acetate strongly correlated with the decrease of ASVs corresponding to members of the *Ruminococcaceae* and *Lachnospiraceae* families, both known as butyrate producers.[84] Of note, one particularly abundant ASV (ASV 2, identified as a member of the *Ruminococcaceae* family and representing in average 20% of the gut microbiota of control mice) exhibited a four-fold decrease in cachectic mice. Interestingly, two ASVs, ASV 10 and ASV 16, identified as members of the *Enterobacteriaceae* family, were negatively correlated with this drop in butyrate and acetate. These results strongly reinforce a mechanism we proposed in 2018 by which a reduction in butyrate production, ensuing from a reduced abundance of butyrate producer families (mainly *Lachnospiraceae* and *Ruminococcaceae*), can contribute to the expansion of *Enterobacteriaceae* in C26 mice through an intestinal glycolytic switch.[80] Butyrate is considered to have various beneficial effects on intestinal health and host metabolism. Among others, it is known to favour intestinal barrier integrity, lower intestinal inflammation, and stimulate glucagon-like peptide 1 production.[85] The changes in the composition of gut microbiota and the subsequent drop in butyrate could participate in the altered intestinal barrier function we reported in C26 mice.[86] The reduced expression of two genes regulated by butyrate in the caecal tissue of C26 mice, namely, *Gcg* coding for the proglucagon, the precursor of glucagon-like peptide 1, and *Zfp148*, a butyrate-inducible zinc finger transcription factor,[87] strongly suggests an impact of butyrate drop on host metabolism (*Figure* S7a and S7b). To overcome the limitation of an ectopic tumour inherent to the C26 model, we also investigated these markers in a mouse model of leukaemia with cachexia, in which we reported an alteration of the gut microbiota composition.[15] Interestingly, the expression of these two genes was also reduced in the proximal colon of leukaemic mice (*Figure* S8a and S8b).

An accelerated intestinal transit contributes to a reduced bacterial metabolism of amino acids and leads to faecal amino acid loss

Amino acids were also significantly altered in C26 CC. Most amino acids displayed a considerable increase in C26 mice (*Figure* 2). Out of the 14 identified amino acids in this compartment, 11 were significantly increased, asparagine showed a trend to increase, aspartate was unchanged, and glutamate was significantly decreased in C26 CC. This increase in most amino acids is surprising considering the reduced food intake and thereby reduced amino acid intake in cachectic mice. We hypothesized that this change could result from an accelerated gastrointestinal transit. Indeed, previous work has reported an inverse correlation between faecal amino acids levels and transit time in healthy humans.[88] In accordance with this hypothesis, we observed that the weight of the caecal and stomach content was significantly reduced in cachectic mice (*Figure* 7A and 7B). A functional test using the Evans Blue dye revealed a two-fold increase in intestinal transit

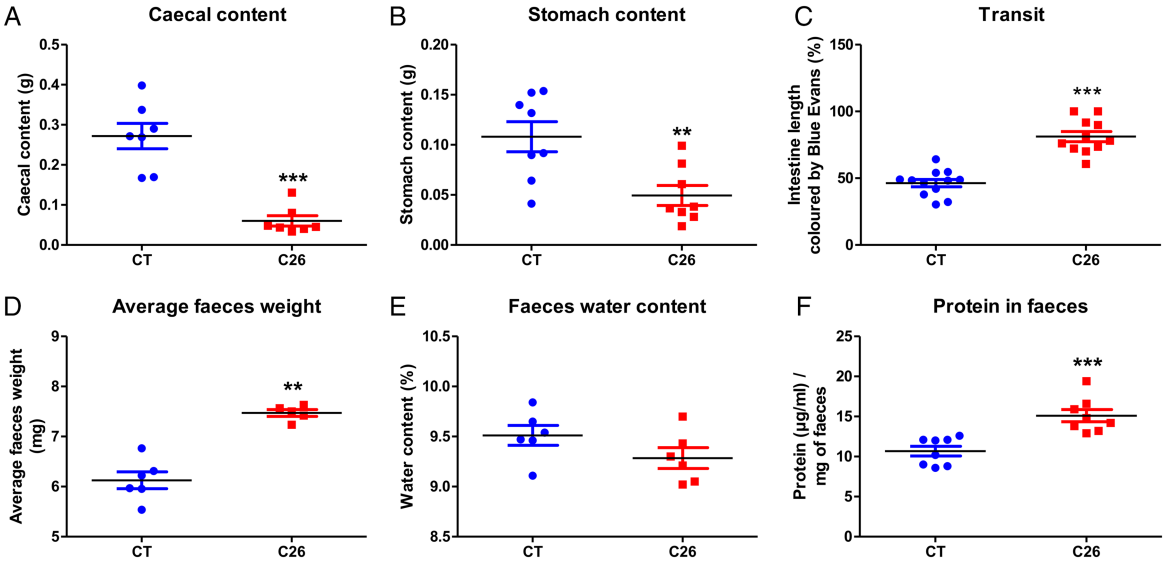

Figure 7 Cachectic (C26) mice present an accelerated transit. (A) Caecal content weight in control (CT) and C26 mice (n = 8 per group). (B) Stomach content (n = 8 per group). (C) Transit time evaluation using Evans Blue (n = 12 per group). (D) Average faeces weight before freeze-drying (n = 6 per group). (E) Faeces water content (n = 6 per group). (F) Faecal protein concentration (n = 8 per group). **P-value <0.01; ***P-value <0.001.

(*Figure* 7C). Finally, we also found an increased average faeces weight that could not be explained by a water content variation but rather by an increased faecal protein concentration (*Figure* 7D–7F). A recent study performed in cachectic rats showed that cachexia accelerated gastric emptying.[89] This study corroborates our finding that gut motility is affected in C26 mice and likely impacts protein and amino acid catabolism in the gastrointestinal tract. Faecal protein content is not commonly reported in cancer cachexia. One paper referred to protein loss in faeces of patients with severe forms of chronic heart failure and cardiac cachexia,[90] whereas another one reported that no protein loss through faeces occurred in elderly patients with cardiac cachexia.[91] Further clinical studies should therefore assess whether protein loss occurs in cancer cachexia.

Changes in transit time were associated to changes in gut microbiota composition.[88] Roager *et al*. reported positive correlations between protein-derived and amino acid-derived bacterial metabolites and Clostridiales member.[88] Coherently, we observed a drastic decrease in the Clostridiales order in C26 mice. In addition, all ASVs showing a strong negative correlation with increased amino acids were members of the Clostridiales order, mainly *Lachnospiraceae* and *Ruminococcaceae* members (*Figure* 6). Using Picrust2, a tool for predicting the functional potential of bacterial metagenomes,[92] we observed the activation of the bacterial degradation pathways of glutamate, the sole amino acid to be decreased in C26 CC (*Table* S4). We found out that four ASVs with a relative abundance between 1% and 6% in C26 mice were negatively correlated to caecal glutamate levels (*Figure* 6) (ASV 8, belonging to the *Lachnospiraceae* family; ASVs 12 and 20 identified as *Flavonifractor* sp.; and ASV 23 belonging to the *Enterobacteriaceae* family) and were part of the top 10 of the ASVs contributing to the glutamate degradation pathways in C26 mice (PWY-5188 and PWY-5918).

Considering the accelerated transit and the changes in the gut microbiota composition, we speculated that most amino acids (with the exception of glutamate) were less metabolized by the cachectic gut microbiota and that this could affect intestinal health. Indeed, metabolites derived from aromatic amino acids (*i.e*. indole derivatives, *p*-cresol, and phenylacetate) can exert positive or negative impacts on the host. A recent work identified 4-cresol, a gut microbiota-derived metabolite of tyrosine and phenylalanine, as an effective regulator of β-cell function.[93] Indole derivatives are tryptophan-derived metabolites and exert many beneficial effects on the host through the activation of the AhR pathway.[94] Concordantly, *Cyp1a1* expression, which reflects

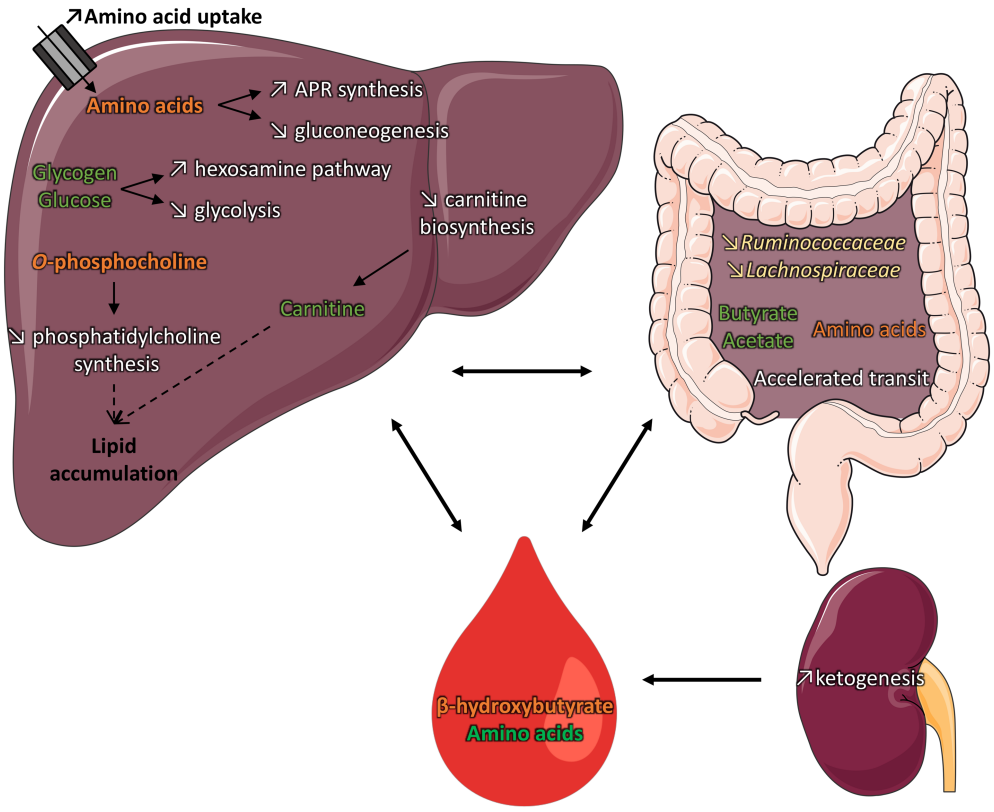

Figure 8 Summary of the main altered pathways identified in cachectic (C26) mice. Significantly increased and decreased metabolites are marked respectively in orange and green. Pathways are presented in white. Dotted lines present the contribution of carnitine and phosphatidylcholine synthesis reductions to lipid accumulation. The figure was produced using Servier Medical ART (www.servier.com).

AhR activity, displayed a seven-fold reduction in the caecal tissue of C26 mice (*Figure* S7c). This reduction in *Cyp1a1* expression was also found in leukaemic mice (*Figure* S8c). This result suggests that tryptophan increase in C26 CC is accompanied by a drop in tryptophan-derived bacterial metabolites and thereby in AhR activity, which importance in intestinal homeostasis maintenance has recently been demonstrated.[94]

Of note, the relationship between bacteria and metabolites is bidirectional. Bacteria can metabolize and produce a various range of metabolites, but these can in turn modulate bacterial growth.[95] Targeted experiments have shown that members of the Firmicutes were generally sensitive to amino acids, reflected by a reduction in their growth *in vitro* when supplemented with amino acids. Members of the Bacteroidetes phylum were mainly insensitive to amino acids supplementation but grew better in media depleted in SCFAs.[95] The results of these *in vitro* experiments correspond to the changes we observed in C26 mice, namely, a decrease in Firmicutes and a trend to an increase in Bacteroidetes with an increase in amino acids and a reduction in SCFAs, showing the mutual impact of altered gut microbiota composition and metabolites in this context.

Changes in bile acids and a reduction in the trimethylamine *N*-oxide pathway characterize C26 mice

Metabolomics analyses in the CC have also pinpointed other changes. Although ^{1}H-NMR is not able to differentiate individual bile acids, we observed an increase in one bile acid subset in C26 CC. A four-fold increase in taurine, the main amino acid conjugated to bile acids in mice, was also observed (*Figure* 2). This increase in taurine could be explained by accelerated transit and/or reduced bacterial metabolism but may also result from a lower hepatic need for bile acid conjugation. Follow-up work revealed that bile acid pathways are deeply altered in cancer cachexia and contribute to hepatic inflammation.[31]

Methylamines (*i.e*. choline, carnitine, and phosphatidylcholine) are degraded by the gut microbiota and further converted in trimethylamine *N*-oxide (TMAO) by the liver.[96] TMAO has been mainly implicated in cardiovascular diseases. As we observed in C26 mice an increase in caecal choline together with a reduction in PV and VC TMAO (*Figure* 2), we concluded that the TMAO pathway is reduced in these mice, excluding a potential contribution of TMAO to cardio-metabolic alterations. Again, such reduction may ensue from a decreased bacterial metabolism and/or accelerated transit.

Conclusions

Integration of an original multi-compartment metabolomics dataset with host transcriptomics data, bacterial metagenomics, and the current literature allowed us to highlight new pathways potentially involved in hepatic alterations associated with cancer cachexia (*Figure* 8). Specifically, we pinpoint that glucose metabolism-related pathways are altered in the C26 model with a reduction in glycolysis and gluconeogenesis and an activation of the hexosamine pathway. We show that amino acids are mainly used for APR protein synthesis by the liver rather than to fuel the TCA cycle and gluconeogenesis. Importantly, reductions in carnitine levels and phosphatidylcholine hepatic formation were identified as new potential contributors to the hepatic steatosis. Another key finding of this work is the major induction of renal ketogenesis leading to β-hydroxybutyrate increase despite the lack of hepatic ketogenic response. By highlighting alterations in liver metabolism that lead to an energy misuse, we strengthen the need to study the liver, an organ often disregarded in cancer cachexia clinical studies. For instance, it becomes of utmost importance to assess hepatic steatosis, alongside carnitine levels, in large cohorts of cachectic patients. Because a drop in carnitine levels has already been reported in patients with cancer cachexia,[68] carnitine supplementation could take part to the multimodal approach to tackle cancer cachexia, not only to increase muscle mass (which has been shown with variable success[97,98]) but also to target hepatic alterations.

This work also brings new insight into the gut microbial activity in cancer cachexia. Many beneficial functions are decreased such as the production of SCFAs and aromatic amino acid metabolites, which may contribute to the altered intestinal homeostasis in these mice (*Figure* 8). One of our most striking findings is undoubtedly the identification of the increased gastrointestinal transit as a key factor shaping the gut microbiota composition in cancer cachexia, which together lead to a faecal loss of proteins and amino acids. The current study paves the way for future mechanistic preclinical studies aiming at determining the contribution of this increased gastrointestinal transit to cachectic features such as muscle atrophy and body weight loss. Finally, our work supports the interest of exploring the gut microbiota composition and activity, in association with the intestinal transit, in cancer patients with and without cachexia. Appropriate stool collection requires a costly logistic organization, and microbiota-centred studies need to be carefully designed to avoid classical bias. However, such efforts will undeniably result in the acquisition of important knowledge on the role played by the gut microbiota in cancer cachexia.

Author contributions

Conception and design of the work were performed by L.B.B. Data collection was carried out by S.A.P, M.M.T., M.S., and L.B.B. Data analysis and interpretation were performed by S.A.P., M.M.T., N.M.D., and L.B.B. The ^{1}H-NMR metabolomics

workflow was designed by S.A.P. with the help of L.B.B. and S. P.C. Guidance on NMR equipment use was provided by N.J. Guidance on biochemical analyses was provided by A.M.N. Access to critical equipment was provided by P.D.C. and N. M.D. Fundings were acquired by N.M.D. and L.B.B. Drafting the article was performed by S.A.P. and L.B.B. All authors carried out the critical revision of the article. All authors approved the version to be published.

Acknowledgements

We thank Dr Paolo E. Porporato and Myriam Hsu (University of Turin) for providing liver samples from LLC mice. We also thank Bouazza Es Saadi, Véronique Allaeys, Isabelle Blave, Alexandra Degraeve, and Halima El-Hamdaoui for skilled assistance and the University of Minnesota Genomics Center for performing the 16S rDNA sequencing. We thank the UCLouvain-LDRI Nuclear and Electron Spin Technologies (NEST) platform for providing easy access and skilled assistance to the NMR spectrometer. All authors of this manuscript comply with the guidelines of ethical authorship and publishing in the *Journal of Cachexia, Sarcopenia and Muscle*.[99]

Conflict of interest

None declared.

Funding

This work was funded by the FSR (Fonds Spéciaux de la Recherche, Université catholique de Louvain, UCLouvain), the Télévie (Intercachectomics consortium), the Louvain Foundation, and the F.R.S.-FNRS (MIS F.4501.20). This work benefitted from the support of the Institut Mérieux through the allocation of the Pharmabiotics Young Investigator Award to L.B.B. L.B.B. and P.D.C are recipients of grants from the Université catholique de Louvain (UCLouvain) (Action de Recherche Concertée ARC19/24-096). N.M.D. is a recipient of grants from the Service Public de Wallonie Économie, Emploi, Recherche (SPW-EER) (convention 1610365, ERA-HDHL co-funded call BioNH 2016), from the Fonds De La Recherche Scientifique - FNRS (F.R.S.-FNRS) [PINT-MULTI R.8013.19 (NEURON-ERANET, call 2019) and PDR T.0068.19], and from the Université catholique de Louvain (UCLouvain) (Action de Recherche Concertée ARC18-23/092). M.M.T. is a research fellow from the FRIA (FRIA, F.R.S.-FNRS). M.S. is a postdoctoral fellow from theAQ10 F.R.S.-FNRS—Télévie. P.D. C. is a senior research associate from the F.R.S.-FNRS.

Online supplementary material

Additional supporting information may be found online in the Supporting Information section at the end of the article.

Figure S1. Cachectic (C26) mice show reduced food intake, body weight loss and muscle atrophy. (a): Body weight evolution (%) in CT and C26 mice. (b): Food intake evolution (%) in control (CT) and C26 mice. (c): Tibialis anterior (TA) and gastrocnemius (GC) muscle weights (% of initial body weight) in CT and C26 mice 10 days after injection. n = 8 per group. *p-value $<$ 0.05.

Figure S2. Principal Component Analyses (PCA) and average control (CT) and cachectic (C26) overlaid ^{1}H-NMR spectra in the four compartments. (a-d): Normalized PCA realised on the intelligent bucketing matrices in the cecal content (CC), portal vein (PV), liver and vena cava (VC) in CT (blue dots) and C26 (red diamonds) mice. (e-h): Average CT (blue) and C26 (red) 1H-NMR spectra in the CC, PV, liver and VC. TSP and water regions were removed. Cecal content: n = 8 per group. Portal vein, liver and vena cava: n = 16 per group.

Figure S3. The hexosamine pathway is activated in the liver of cachectic (C26) mice. (a): Schematic view of the hexosamine pathway in the liver of control (CT) and C26 mice. The metabolite in green is significantly decreased in C26 mice; the metabolite in orange is significantly increased in C26 mice (n = 16 per group). The relative expression of the enzymes of the pathway are expressed in counts (n = 8 per group). All changes, including the rate limiting enzyme *Gfpt1,* are significant (q-value $<$ 0.01). (b): Expression level of *Xbp1s,* coding for the spliced X-Box Binding Protein 1, in the liver of CT and C26 mice (n = 8 per group). *p-value $<$ 0.05; ***q-value $<$ 0.001.

Figure S4. Hepatic ketogenic response is activated in healthy mice enduring food restriction and kidney ketogenic response is activated in cachectic (C26) mice. (a): β-hydroxybutyrate levels in the systemic circulation of control (CT), C26, pair-fed to CT (PF-CT) and pair-fed to C26 (PF-C26) mice. (b): β-hydroxybutyrate levels in the liver of CT, C26, PF-CT and PF-C26 mice. (c): Relative expression of *Hmgcs2* in the liver of CT, C26, PF-CT and PF-C26 mice. (d): Relative expression of *Hmgcs2* in the kidney of CT and C26. n = 7–8 per group. * comparison between CT and C26 groups; # comparison between PF-CT and PF-C26 groups. *p-value $<$ 0.05; ***p-value $<$ 0.001; ##p-value $<$ 0.01; ###p-value $<$ 0.001.

Figure S5. LLC mice display similar alterations in hepatic metabolism to C26 mice. (a): *Pck1* and *G6pc* relative expression, two key gluconeogenic enzymes. (b): *Slc3a1*, *Slc7a5*, Slc43a1 relative expression, three amino acid transporters. (c): S*aa1*, *Saa2* and *Apcs* relative expression, the three main acute phase response proteins in mice. (d): *Cps1* relative

expression, the key enzyme of urea synthesis. (e): *Bbox1* relative expression, the key enzyme of carnitine biosynthesis. (f): *Pcyt1a* and *Chpt1* relative expression, two enzymes involved in *O*-phosphocholine to phosphatidylcholine transformation. (g): *Hmgcs2* relative expression, the key enzyme of ketogenesis and β-hydroxybutyrate concentration in the liver. n = 6 per group. *p-value $<$ 0.05; **p-value $<$ 0.01.

Figure S6. Gut microbiota composition is altered in cachectic (C26) mice. (a-b): Principal coordinate analysis of the (a) Bray-Curtis and (b) Morisita-Horn β-diversity indexes computed based on the ASV table. (c): Stacked plot displaying the mean of the relative abundance of each phylum in CT and C26 mice. (d) Stacked plot displaying the mean of the relative abundance of each family in CT and C26 mice. n = 8 per group. *q-value $<$ 0.05.

Figure S7. *Gcg*, *Zfp148* and *Cyp1a1* expressions are decreased in cachectic (C26) cecal tissue. n = 8 per group. ***p-value $<$ 0.001.

Figure S8. *Gcg*, *Zfp148* and *Cyp1a1* expressions are decreased in leukaemic BaF mice. (a): *Gcg* relative expression in the proximal colon of CT and BaF mice. (b): *Zfp148* relative expression in the proximal colon of CT and BaF mice. (c): *Cyp1a1* relative expression in the ileum of CT and BaF mice. n = 8 per group. *p-value $<$ 0.05; **p-value $<$ 0.01; ***p-value $<$ 0.001.

Table S1. Full ^{1}H-NMR chemical shift data for metabolites identified in the cecal content (CC), portal vein (PV), liver (L) and vena cava (VC). The numbering/nomenclature of compounds follows the IUPAC system. s, singlet; d, doublet, dd, doublet of doublets; t, triplet; m, multiplet.

Table S2. Primers used in the study.

Table S3. Fold changes for each identified metabolite in the four compartments.

Each metabolite is associated with a number for the correspondance with the correlation circle plots in Figure 1. Cecal content: n = 8 per group. Portal vein, liver and vena cava: n = 16 per group. *q-value $<$ 0.05; **q-value $<$ 0.01; ***q-value $<$ 0.001.

Table S4. Glutamate biosynthesis and degradation pathways are predicted to be affected in the gut microbiome of cachectic mice. n = 8 per group.

Table S5. Amplicon sequence variants (ASVs) average relative abundance in control (CT) and cachectic (C26) mice. ASVs with an average relative abundance superior to 0.1% in at least one group were selected for canonical partial least squares analyses. For these, lowest taxon identification was performed using the RDP database. n = 8 per group.

Data S1. Supporting information

References

1. Baracos VE, Martin L, Korc M, Guttridge DC, Fearon KCH. Cancer-associated cachexia. *Nat Rev Dis Primers* 2018;**4**:17105.
2. Rohm M, Zeigerer A, Machado J, Herzig S. Energy metabolism in cachexia. *EMBO Rep* 2019;**20**.
3. Fearon K, Strasser F, Anker SD, Bosaeus I, Bruera E, Fainsinger RL, et al. Definition and classification of cancer cachexia: an international consensus. *Lancet Oncol* 2011;**12**:489–495.
4. Schmidt SF, Rohm M, Herzig S, Berriel Diaz M. Cancer cachexia: more than skeletal muscle wasting. *Trends Cancer* 2018;**4**:849–860.
5. Holroyde CP, Gabuzda TG, Putnam RC, Paul P, Reichard GA. Altered glucose metabolism in metastatic carcinoma. *Cancer Res* 1975;**35**:3710–3714.
6. Falconer JS, Fearon KC, Plester CE, Ross JA, Carter DC. Cytokines, the acute-phase response, and resting energy expenditure in cachectic patients with pancreatic cancer. *Ann Surg* 1994;**219**:325–331.
7. Dumas JF, Goupille C, Julienne CM, Pinault M, Chevalier S, Bougnoux P, et al. Efficiency of oxidative phosphorylation in liver mitochondria is decreased in a rat model of peritoneal carcinosis. *J Hepatol* 2011;**54**:320–327.
8. Berriel Diaz M, Krones-Herzig A, Metzger D, Ziegler A, Vegiopoulos A, Klingenspor M, et al. Nuclear receptor cofactor receptor interacting protein 140 controls hepatic triglyceride metabolism during wasting in mice. *Hepatology* 2008;**48**:782–791.
9. Jones A, Friedrich K, Rohm M, Schafer M, Algire C, Kulozik P, et al. TSC22D4 is a molecular output of hepatic wasting metabolism. *EMBO Mol Med* 2013;**5**:294–308.
10. Tilg H, Zmora N, Adolph TE, Elinav E. The intestinal microbiota fuelling metabolic inflammation. *Nat Rev Immunol* 2020;**20**:40–54.
11. Delzenne NM, Knudsen C, Beaumont M, Rodriguez J, Neyrinck AM, Bindels LB. Contribution of the gut microbiota to the regulation of host metabolism and energy balance: a focus on the gut-liver axis. *Proc Nutr Soc* 2019;**78**:319–328.
12. Oliphant K, Allen-Vercoe E. Macronutrient metabolism by the human gut microbiome: major fermentation by-products and their impact on host health. *Microbiome* 2019;**7**:91.
13. Dzutsev A, Badger JH, Perez-Chanona E, Roy S, Salcedo R, Smith CK, et al. Microbes and cancer. *Annu Rev Immunol* 2017;**35**:199–228.
14. Helmink BA, Khan MAW, Hermann A, Gopalakrishnan V, Wargo JA. The microbiome, cancer, and cancer therapy. *Nat Med* 2019;**25**:377–388.
15. Bindels LB, Neyrinck AM, Claus SP, Le Roy CI, Grangette C, Pot B, et al. Synbiotic approach restores intestinal homeostasis and prolongs survival in leukaemic mice with cachexia. *ISME J* 2016;**10**:1456–1470.
16. Bindels LB, Neyrinck AM, Salazar N, Taminiau B, Druart C, Muccioli GG, et al. Non digestible oligosaccharides modulate the gut microbiota to control the development of leukemia and associated cachexia in mice. *PLoS One.* 2015;**10**:e0131009.
17. Bindels LB, Porporato P, Dewulf EM, Verrax J, Neyrinck AM, Martin JC, et al. Gut microbiota-derived propionate reduces cancer cell proliferation in the liver. *Br J Cancer* 2012;**107**:1337–1344.
18. Emwas AHM, Salek RM, Griffin JL, Merzaban J. NMR-based metabolomics in human disease diagnosis: applications, limitations, and recommendations. *Metabolomics.* 2013;**9**:1048–1072.
19. Visconti A, Le Roy CI, Rosa F, Rossi N, Martin TC, Mohney RP, et al. Interplay between the human gut microbiome and host metabolism. *Nat Commun* 2019;**10**:4505.
20. Hoyles L, Fernandez-Real JM, Federici M, Serino M, Abbott J, Charpentier J, et al. Molecular phenomics and metagenomics of hepatic steatosis in non-diabetic obese women. *Nat Med* 2018;**24**:1070–1080.
21. Gallagher IJ, Jacobi C, Tardif N, Rooyackers O, Fearon K. Omics/systems

biology and cancer cachexia. *Semin Cell Dev Biol* 2016;**54**:92–103.
22. Pin F, Barreto R, Couch ME, Bonetto A, O'Connell TM. Cachexia induced by cancer and chemotherapy yield distinct perturbations to energy metabolism. *J Cachexia Sarcopenia Muscle* 2019;**10**: 140–154.
23. O'Connell TM, Ardeshirpour F, Asher SA, Winnike JH, Yin X, George J, et al. Metabolomic analysis of cancer cachexia reveals distinct lipid and glucose alterations. *Metabolomics* 2008; **4**:216–225.
24. Der-Torossian H, Wysong A, Shadfar S, Willis MS, McDunn J, Couch ME. Metabolic derangements in the gastrocnemius and the effect of Compound A therapy in a murine model of cancer cachexia. *J Cachexia Sarcopenia Muscle* 2013;**4**:145–155.
25. Lautaoja JH, Lalowski M, Nissinen TA, Hentila J, Shi Y, Ritvos O, et al. Muscle and serum metabolomes are dysregulated in colon-26 tumor-bearing mice despite amelioration of cachexia with activin receptor type 2B ligand blockade. *Am J Physiol Endocrinol Metab* 2019;**316**: E852–E865.
26. De Winter BY, De Man JG, Seerden TC, Depoortere I, Herman AG, Peeters TL, et al. Effect of ghrelin and growth hormone-releasing peptide 6 on septic ileus in mice. *Neurogastroenterol Motil* 2004;**16**:439–446.
27. Bindels LB, Beck R, Schakman O, Martin JC, De Backer F, Sohet FM, et al. Restoring specific lactobacilli levels decreases inflammation and muscle atrophy markers in an acute leukemia mouse model. *PLoS One* 2012;**7**:e37971.
28. Beckonert O, Keun HC, Ebbels TM, Bundy J, Holmes E, Lindon JC, et al. Metabolic profiling, metabolomic and metabonomic procedures for NMR spectroscopy of urine, plasma, serum and tissue extracts. *Nat Protoc* 2007;**2**:2692–2703.
29. Sousa SAA, Magalhães A, Ferreira MMC. Optimized bucketing for NMR spectra: three case studies. *Chemom Intel Lab Syst* 2013;**122**:93–102.
30. Wishart DS, Feunang YD, Marcu A, Guo AC, Liang K, Vazquez-Fresno R, et al. HMDB 4.0: the human metabolome database for 2018. *Nucleic Acids Res* 2018;**46**: D608–D617.
31. Thibaut MM, Sboarina M, Roumain M, Pötgens SA, Neyrinck AM, Destrée F, et al. Inflammation-induced cholestasis in cancer cachexia. *Journal of Cachexia, Sarcopenia and Muscle* 2020.
32. Bolger AM, Lohse M, Usadel B. Trimmomatic: a flexible trimmer for Illumina sequence data. *Bioinformatics* 2014;**30**:2114–2120.
33. Dobin A, Davis CA, Schlesinger F, Drenkow J, Zaleski C, Jha S, et al. STAR: ultrafast universal RNA-seq aligner. *Bioinformatics* 2013;**29**:15–21.
34. Lawrence M, Huber W, Pages H, Aboyoun P, Carlson M, Gentleman R, et al. Software for computing and annotating genomic ranges. *PLoS Comput Biol* 2013;**9**:e1003118.
35. Love MI, Huber W, Anders S. Moderated estimation of fold change and dispersion for RNA-seq data with DESeq2. *Genome Biol* 2014;**15**:550.
36. Edgar RC. UNOISE2: improved error-correction for Illumina 16S and ITS amplicon sequencing. *bioRxiv.* 2016: 081257.
37. Breton J, Tirelle P, Hasanat S, Pernot A, L'Huillier C, do Rego JC, et al. Gut microbiota alteration in a mouse model of Anorexia Nervosa. *Clin Nutr* 2020;**40**:181–189.
38. Suriano F, Bindels LB, Verspreet J, Courtin CM, Verbeke K, Cani PD, et al. Fat binding capacity and modulation of the gut microbiota both determine the effect of wheat bran fractions on adiposity. *Sci Rep* 2017;**7**:5621.
39. Team RDC. R: a language and environment for statistical computing. R Foundation for Statistical Computing, Vienna, Austria. ISBN 3–900051–07-0, URL http://www.R-project.org/. 2012.
40. Benjamini Y, Hochberg Y. Controlling the false discovery rate: a practical and powerful approach to multiple testing. *J R Statist Soc B* 1995;**57**:289–300.
41. Rohart F, Gautier B, Singh A, Lê Cao KA. mixOmics: an R package for 'omics feature selection and multiple data integration. *PLoS Computational Biology* 2017;**13**:e1005752.
42. Lemon J. Plotrix: a package in the red light district of R. *R-News* 2006;**6**:8–12.
43. Keitt TH. Coherent ecological dynamics induced by large-scale disturbance. *Nature* 2008;**454**:331–334.
44. French JP. autoimage: multiple heat maps for projected coordinates. *The R Journal* 2017;**9**:284–297.
45. Wickham H, Averick M, Bryan J, Chang W, McGowan L, François R, et al. Welcome to the tidyverse. *Journal of Open Source Software* 2019;**4**:1686.
46. Lê Cao K-A, Martin PGP, Robert-Granié C, Besse P. Sparse canonical methods for biological data integration: application to a cross-platform study. *BMC Bioinformatics* 2009;**10**:34.
47. González I, Cao KAL, Davis MJ, Déjean S. Visualising associations between paired 'omics' data sets. *BioData Mining* 2012;**5**.
48. Hutton JC, O'Brien RM. Glucose-6-phosphatase catalytic subunit gene family. *J Biol Chem* 2009;**284**:29241–29245.
49. Khamoui AV, Tokmina-Roszyk D, Rossiter HB, Fields GB, Visavadiya NP. Hepatic proteome analysis reveals altered mitochondrial metabolism and suppressed acyl-CoA synthetase-1 in colon-26 tumor-induced cachexia. *Physiol Genomics* 2020;**52**:203–216.
50. Chen J, Yu Y, Gao J, Yang S. UDP-glucose dehydrogenase: the first-step oxidation is an NAD^+-dependent bimolecular nucleophilic substitution reaction (S_N2). *Int J Biol Sci* 2019;**15**:341–350.
51. Buckley DB, Klaassen CD. Tissue- and gender-specific mRNA expression of UDP-glucuronosyltransferases (UGTs) in mice. *Drug Metab Dispos* 2007;**35**: 121–127.
52. Roy A, Kumar A. ER stress and unfolded protein response in cancer cachexia. *Cancers (Basel)* 2019;**11**:1929.
53. Hentila J, Nissinen TA, Korkmaz A, Lensu S, Silvennoinen M, Pasternack A, et al. Activin receptor ligand blocking and cancer have distinct effects on protein and redox homeostasis in skeletal muscle and liver. *Front Physiol* 2018;**9**:1917.
54. Wang ZV, Deng Y, Gao N, Pedrozo Z, Li DL, Morales CR, et al. Spliced X-box binding protein 1 couples the unfolded protein response to hexosamine biosynthetic pathway. *Cell* 2014;**156**:1179–1192.
55. Werner C, Doenst T, Schwarzer M. Chapter 4—metabolic pathways and cycles. In Schwarzer M, Doenst T, eds. *The Scientist's Guide to Cardiac Metabolism*. Boston: Academic Press; 2016. 39–55.
56. Connelly MA, Otvos JD, Shalaurova I, Playford MP, Mehta NN. GlycA, a novel biomarker of systemic inflammation and cardiovascular disease risk. *J Transl Med* 2017;**15**:219.
57. Argilés JM, Stemmler B, López-Soriano FJ, Busquets S. Inter-tissue communication in cancer cachexia. *Nat Rev Endocrinol* 2019;**15**:9–20.
58. Argiles JM, Campos N, Lopez-Pedrosa JM, Rueda R, Rodriguez-Manas L. Skeletal muscle regulates metabolism via interorgan crosstalk: roles in health and disease. *J Am Med Dir Assoc* 2016;**17**:789–796.
59. Szalai AJ, van Ginkel FW, Dalrymple SA, Murray R, McGhee JR, Volanakis JE. Testosterone and IL-6 requirements for human C-reactive protein gene expression in transgenic mice. *J Immunol* 1998;**160**:5294–5299.
60. de Blaauw I, Deutz NE, Boers W, von Meyenfeldt MF. Hepatic amino acid and protein metabolism in non-anorectic, moderately cachectic tumor-bearing rats. *J Hepatol* 1997;**26**:396–408.
61. Fearon KC, McMillan DC, Preston T, Winstanley FP, Cruickshank AM, Shenkin A. Elevated circulating interleukin-6 is associated with an acute-phase response but reduced fixed hepatic protein synthesis in patients with cancer. *Ann Surg* 1991;**213**:26–31.
62. Fearon KC, Barber MD, Falconer JS, McMillan DC, Ross JA, Preston T. Pancreatic cancer as a model: inflammatory mediators, acute-phase response, and cancer cachexia. *World J Surg* 1999;**23**:584–588.
63. Nissinen TA, Hentila J, Penna F, Lampinen A, Lautaoja JH, Fachada V, et al. Treating cachexia using soluble ACVR2B improves survival, alters mTOR localization, and attenuates liver and spleen responses. *J Cachexia Sarcopenia Muscle* 2018;**9**: 514–529.
64. Czaja MJ, Ding WX, Donohue TM Jr, Friedman SL, Kim JS, Komatsu M, et al. Functions of autophagy in normal and

diseased liver. *Autophagy* 2013;**9**: 1131–1158.
65. Petrasek J, Erhartova D, Levine B. Protective effect of SMAD-specific E3 ubiquitin protein ligase 1 in alcoholic steatohepatitis in mice. *Hepatol Commun* 2019;**3**:1450–1458.
66. Rosa-Caldwell ME, Brown JL, Lee DE, Wiggs MP, Perry RA Jr, Haynie WS, et al. Hepatic alterations during the development and progression of cancer cachexia. *Appl Physiol Nutr Metab* 2020;**45**: 500–512.
67. Nicklin P, Bergman P, Zhang B, Triantafellow E, Wang H, Nyfeler B, et al. Bidirectional transport of amino acids regulates mTOR and autophagy. *Cell* 2009;**136**:521–534.
68. Silverio R, Laviano A, Rossi Fanelli F, Seelaender M. L-Carnitine and cancer cachexia: clinical and experimental aspects. *J Cachexia Sarcopenia Muscle* 2011;**2**: 37–44.
69. Liu S, Wu HJ, Zhang ZQ, Chen Q, Liu B, Wu JP, et al. L-Carnitine ameliorates cancer cachexia in mice by regulating the expression and activity of carnitine palmityl transferase. *Cancer Biol Ther* 2011;**12**: 125–130.
70. Goncalves DC, Lira FS, Yamashita AS, Carnevali Junior LC, Eder R, Laviano A, et al. Liver lipid metabolism disruption in cancer cachexia is aggravated by cla supplementation-induced inflammation. *Clin Nutr* 2019;**38**:2219–2230.
71. Jiang F, Zhang Z, Zhang Y, Pan X, Yu L, Liu S. L-Carnitine ameliorates cancer cachexia in mice partly via the carnitine palmitoyltransferase-associated PPAR-γ signaling pathway. *Oncol Res Treat* 2015;**38**:511–516.
72. Silverio R, Laviano A, Rossi Fanelli F, Seelaender M. L-Carnitine induces recovery of liver lipid metabolism in cancer cachexia. *Amino Acids* 2012;**42**:1783–1792.
73. Vaz FM, Wanders RJ. Carnitine biosynthesis in mammals. *Biochem J* 2002;**361**: 417–429.
74. Li Z, Vance DE. Phosphatidylcholine and choline homeostasis. *J Lipid Res* 2008;**49**:1187–1194.
75. Heijboer AC, Donga E, Voshol PJ, Dang ZC, Havekes LM, Romijn JA, et al. Sixteen hours of fasting differentially affects hepatic and muscle insulin sensitivity in mice. *J Lipid Res* 2005;**46**:582–588.
76. Flint TR, Janowitz T, Connell CM, Roberts EW, Denton AE, Coll AP, et al. Tumor-induced IL-6 reprograms host metabolism to suppress anti-tumor immunity. *Cell Metab* 2016;**24**:672–684.
77. Der-Torossian H, Asher SA, Winnike JH, Wysong A, Yin X, Willis MS, et al. Cancer cachexia's metabolic signature in a murine model confirms a distinct entity. *Metabolomics.* 2013;**9**:730–739.
78. Takagi A, Kume S, Kondo M, Nakazawa J, Chin-Kanasaki M, Araki H, et al. Mammalian autophagy is essential for hepatic and renal ketogenesis during starvation. *Sci Rep* 2016;**6**:18944.
79. Owen OE, Felig P, Morgan AP, Wahren J, Cahill GF Jr. Liver and kidney metabolism during prolonged starvation. *J Clin Invest* 1969;**48**:574–583.
80. Potgens SA, Brossel H, Sboarina M, Catry E, Cani PD, Neyrinck AM, et al. *Klebsiella oxytoca* expands in cancer cachexia and acts as a gut pathobiont contributing to intestinal dysfunction. *Sci Rep* 2018;**8**: 12321.
81. Callahan BJ, McMurdie PJ, Holmes SP. Exact sequence variants should replace operational taxonomic units in marker-gene data analysis. *ISME J* 2017;**11**:2639–2643.
82. Louis P, Hold GL, Flint HJ. The gut microbiota, bacterial metabolites and colorectal cancer. *Nat Rev Microbiol* 2014;**12**: 661–672.
83. Alexander C, Swanson KS, Fahey GC, Garleb KA. Perspective: physiologic importance of short-chain fatty acids from nondigestible carbohydrate fermentation. *Adv Nutr* 2019;**10**:576–589.
84. Rios-Covian D, Ruas-Madiedo P, Margolles A, Gueimonde M, de Los Reyes-Gavilan CG, Salazar N. Intestinal short chain fatty acids and their link with diet and human health. *Front Microbiol* 2016;**7**:185.
85. Dalile B, Van Oudenhove L, Vervliet B, Verbeke K. The role of short-chain fatty acids in microbiota–gut–brain communication. *Nat Rev Gastroenterol Hepatol* 2019;**16**:461–478.
86. Bindels LB, Neyrinck AM, Loumaye A, Catry E, Walgrave H, Cherbuy C, et al. Increased gut permeability in cancer cachexia: mechanisms and clinical relevance. *Oncotarget* 2018;**9**:18224–18238.
87. Essien BE, Grasberger H, Romain RD, Law DJ, Veniaminova NA, Saqui-Salces M, et al. ZBP-89 regulates expression of *tryptophan hydroxylase I* and mucosal defense against *Salmonella typhimurium* in mice. *Gastroenterology* 2013;**144**: 1466–1477.
88. Roager HM, Hansen LB, Bahl MI, Frandsen HL, Carvalho V, Gobel RJ, et al. Colonic transit time is related to bacterial metabolism and mucosal turnover in the gut. *Nat Microbiol* 2016;**1**:16093.
89. de Sousa Cavalcante ML, Silva MS, Cavalcante AKM, de Oliveira Santos R, Nunes DDT, Busquets S, et al. Win 55,212-2, atenolol and subdiaphragmatic vagotomy prevent acceleration of gastric emptying induced by cachexia via Yoshida-AH-130 cells in rats. *Eur J Pharmacol* 2020;**877**:173087.
90. Arutyunov GP, Kostyukevich OI, Serov RA, Rylova NV, Bylova NA. Collagen accumulation and dysfunctional mucosal barrier of the small intestine in patients with chronic heart failure. *Int J Cardiol* 2008;**125**:240–245.
91. King D, Smith ML, Lye M. Gastro-intestinal protein loss in elderly patients with cardiac cachexia. *Age Ageing* 1996;**25**: 221–223.
92. Douglas GM, Maffei VJ, Zaneveld J, Yurgel SN, Brown JR, Taylor CM, *et al*. PICRUSt2: an improved and customizable approach for metagenome inference. *bioRxiv*. 2020:672295.
93. Brial F, Alzaid F, Sonomura K, Kamatani Y, Meneyrol K, Le Lay A, et al. The natural metabolite 4-cresol improves glucose homeostasis and enhances β-cell function. *Cell Rep* 2020;**30**:2306–2320, e2305.
94. Agus A, Planchais J, Sokol H. Gut microbiota regulation of tryptophan metabolism in health and disease. *Cell Host Microbe* 2018;**23**:716–724.
95. Tramontano M, Andrejev S, Pruteanu M, Klunemann M, Kuhn M, Galardini M, et al. Nutritional preferences of human gut bacteria reveal their metabolic idiosyncrasies. *Nat Microbiol* 2018;**3**:514–522.
96. Fennema D, Phillips IR, Shephard EA. Trimethylamine and trimethylamine *N*-oxide, a flavin-containing monooxygenase 3 (FMO3)-mediated host-microbiome metabolic axis implicated in health and disease. *Drug Metab Dispos* 2016;**44**:1839–1850.
97. Prado CM, Purcell SA, Laviano A. Nutrition interventions to treat low muscle mass in cancer. *J Cachexia Sarcopenia Muscle* 2020;**11**:366–380.
98. Mitchell T, Clarke L, Goldberg A, Bishop KS. Pancreatic cancer cachexia: the role of nutritional interventions. *Healthcare (Basel)* 2019;**7**:89
99. von Haehling S, Morley JE, Coats AJS, Anker SD. Ethical guidelines for publishing in the *Journal of Cachexia, Sarcopenia and Muscle*: update 2019. *J Cachexia Sarcopenia Muscle* 2019;**10**:1143–1145.
100. Kandasamy P, Gyimesi G, Kanai Y, Hediger MA. Amino acid transporters revisited: new views in health and disease. *Trends Biochem Sci* 2018;**43**:752–789.